Journal of Ship Research, Vol. 31, No. 2, June 1987, pp. 107–124

The Surface Singularity Method Applied to Partially Cavitating Hydrofoils

James S. Uhlman, Jr[1]

The surface singularity or boundary integral method is formulated numerically for the problem of the fully nonlinear potential flow past a partially cavitating hydrofoil. An iterative scheme is employed to locate the cavity surface. Upon convergence the exact boundary conditions are satisfied on all portions of the foil-cavity boundary. The effects of hydrofoil section thickness and camber on cavity volume are investigated. The results are compared with those generated by a numerical linear theory, which includes the effect of section thickness, and with Tulin and Hsu's "short cavity" theory. Both section thickness and camber are shown to have significant effects on cavity volume.

Introduction

AS SHIPS have become larger and propeller loadings greater over the course of this century, the phenomenon of cavitation on marine propellers has become more the rule than the exception. This fact has attendant with it many problems. Among these is the radiated pressure field associated with unsteady propeller cavitation. This has been shown to be the dominant contributor to unsteady hull forces and has caused severe noise and vibration problems on some ships. A related problem is that of underwater noise. The largest source of underwater noise from a ship is usually a cavitating propeller. The magnitude and monopole nature of the radiated pressure field makes use of underwater acoustic sensors difficult.

Due to problems such as these, a thorough understanding of cavitation is desirable if we are to try to alleviate or lessen the severity of the impact of cavitation.

Many forms of cavitation exist, such as bubble cavitation, cloud cavitation and sheet cavitation. Excellent reviews of the general state of knowledge in the area of cavitation may be found in such works as Birkhoff and Zarantonello [1],[2] Eisenberg and Tulin [2], Gilbarg [3], Gurevich [4,5], Hsu [6], Knapp et al [7], Plesset [8], Robertson and Wislicenus [9], Tulin [10], Tulin and Hsu [11], Wehausen [12], Wu [13,14] and Yegorov et al [15].

The problem of lifting-surface sheet cavitation, which is addressed here, is a free-streamline problem; that is, there is a flow boundary whose location must be determined as part of the solution. Such problems were first addressed by Helmholtz and Kirchoff, roughly a century ago, via a technique from the theory of functions of a complex variable called the hodograph. The problem they solved was essentially that of a supercavitating flat plate at zero cavitation number. Levi-Civita extended their technique to include the flow past curved bodies, and others applied the technique to numerous, now classical, jet and cavity flow problems [1].

The next step was the introduction of models that allow for finite cavitation numbers and hence finite cavities. These models assume supercavitation and may be characterized by the manner in which the cavity is terminated. Among these is the Riabouchinsky cavity termination and the physically realistic reentrant jet model [16–19]. These models are all fully nonlinear, satisfying the exact kinematic and dynamic boundary conditions on the cavity surface. The analytical difficulties inherent in these models are enormous, and preclude their use as an engineering tool. A better tool was needed.

In 1953 Tulin [20] developed a linearized theory for zero cavitation number. There followed a period during which the theory was extensively applied and extended. In 1959 Geurst [21,22] introduced the linearized theory for partially cavitating hydrofoils at finite cavitation numbers and followed it, the next year [23], with the linearized theory for supercavitating hydrofoils at finite cavitation numbers. The effect of thickness on plano-convex foils was investigated, in a linearized sense, by Wade [24] in 1967.

Three-dimensional effects were the next aspect to be taken into account. In 1971 Leehey [25] introduced the theory of supercavitating hydrofoils of finite span. This theory uses the method of matched asymptotic expansions to match Geurst's [23] two-dimensional result to the outer three-dimensional flow with inverse aspect ratio as the expansion parameter. Following similar lines, the theory of a partially cavitating hydrofoil of finite span was presented by Uhlman [26] in 1978.

The large-scale use of computers brought about the next and present era of solutions to cavity flow problems. Golden [27] began this trend by numerically reproducing Geurst's [21] linear theory for flat plates in 1975. The leap to three-dimensional problems was made shortly thereafter by Jiang [28]. In 1977 Jiang produced an unsteady numerical lifting-surface theory for supercavitating hydrofoils of finite span using a vortex-source lattice technique. This lattice technique was put to perhaps its ultimate test in 1979, when Lee [29] used it to solve the problem of an unsteady, cavitating marine propeller.

Obviously, the study of cavitating flows has progressed greatly in the last 100 years. However, there are still many unanswered questions in this field, even if we restrict ourselves to the potential-flow model. Most of the work done in the past 20 years has utilized some form of linearized approximation. This is true of the numerical approaches mentioned above. However, due to the analytical intractability of the nonlinear models, very little comparison of nonlinear and linear results has taken place, leaving the accuracy and limitations of the linear theory uncertain and occasionally suspect. There are also questions concerning nonlinear effects. For example, what are they, how significant can they be, and could an accurate knowledge of them be used to engineering advantage?

To answer such questions some form of tractable nonlinear model is needed. Fortunately, numerical techniques are now

[1] Gould Defense Systems, Inc., Ocean Systems Division, Middletown, Rhode Island.

[2] Numbers in brackets designate References at end of paper.

Manuscript received at SNAME headquarters December 20, 1985; revised manuscript received May 2, 1986.

available which allow one to make use of today's high-speed computers in the solution of the exact, nonlinear problem.

These numerical techniques stem from theorems in potential-flow theory which state that the solution of a Neumann, Dirichlet, or mixed boundary condition problem may be expressed as an integral of appropriate singularities distributed over the boundary of the flow field. Due to these theorems, these techniques are frequently referred to as boundary-integral or surface-singularity techniques. Following the 1966 paper by Hess and Smith [30] on the calculation of potential flows about arbitrary bodies, the range of applications of these techniques expanded rapidly. Hess [31,32] soon presented procedures for steady two-dimensional lifting flows and in 1978 Basu and Hancock [33] introduced a technique for handling the unsteady case. By 1976 Bristow [34] had succeeded in developing an iterative technique for the design problem, the design problem being of interest here because the techniques employed are closely related to those required for the solution of nonlinear free-streamline problems.

Giesing and Smith in 1967 [35] had already applied a surface singularity technique to the problem of two-dimensional hydrofoils beneath a free surface, but had only imposed the linear free-surface boundary condition. Results satisfying the nonlinear free-surface boundary condition were presented by Hess [36] in 1977 at the same conference where Larock [37] introduced similar techniques applied to jet flows. Finally, in 1981 Pellone and Rowe [38] applied similar techniques to two- and three-dimensional supercavitating hydrofoil problems.

A need presently exists to validate our working tools, which are based, by and large, on lifting-surface theory, and to investigate effects such as camber and thickness in exact nonlinear models. In an attempt to meet these needs, an exact nonlinear numerical model for the partially cavitating flow about two-dimensional hydrofoils is presented herein. It uses a surface vorticity technique in conjunction with an iterative procedure to generate the cavity shape. The effects of thickness, leading-edge radius, and camber are investigated and compared with linear theory and the thin-cavity theory of Tulin and Hsu [39]. The results are found to differ significantly.

Mathematical formulation

Consider the unbounded steady irrotational flow of an inviscid, incompressible liquid past a cavitating hydrofoil (Fig. 1). The flow is then a potential flow and hence possesses a potential function, Φ, which in the flow field satisfies

$$\nabla^2\Phi = 0 \tag{1}$$

One can define a disturbance potential, ϕ, by

$$\Phi = \vec{U}_\infty \cdot \vec{r} + \phi \tag{2}$$

where $\vec{U}_\infty$ is the freestream velocity and $\vec{r} = x\vec{i} + y\vec{j}$ is the position vector. If one nondimensionalizes on $|\vec{U}_\infty|$ and c, where c is the chord length of the foil, then redefining all terms as nondimensional, except where stated otherwise, one finds that

$$\vec{U}_\infty = \cos(\alpha)\vec{i} + \sin(\alpha)\vec{j} \tag{3}$$

Here α is the angle of attack of the foil defined with respect to the nose-tail line. Equations (1) and (2) still hold, yet now in nondimensional form.

Defining the surface vorticity, γ, to be positive for clockwise-induced flow, it can be easily shown (see the Appendix), that

Nomenclature

c = chord length
C = integration contour
C = foil-cavity boundary
C_c = cavity boundary contour
C_p = pressure coefficient $= \dfrac{p - p_\infty}{\frac{1}{2}\rho U_\infty^2}$
C_L = lift coefficient $= \dfrac{L}{\frac{1}{2}\rho U_\infty^2 c}$
C_M = moment coefficient $= \dfrac{M}{\frac{1}{2}\rho U_\infty^2 c^2}$
C_D = drag coefficient $= \dfrac{D}{\frac{1}{2}\rho U_\infty^2 c}$
D^+ = region exterior to foil-cavity boundary
D^- = region interior to foil-cavity boundary
∂D = foil-cavity boundary
dL = elemental lift force
dM = elemental moment
dD = elemental drag force
$g(x)$ = cavity shape
g_ℓ = cavity surface element end-point ordinate
$h^+(x)$ = shape of upper surface of hydrofoil
$h^-(x)$ = shape of lower surface of hydrofoil
$\hat{n}$ = normal vector, pointing into fluid
n_x, n_y = cartesian components of normal vector
$\hat{n}_k$ = normal vector for kth surface element
n_{x_k}, n_{y_k} = cartesian components of normal vector for kth surface element
N = number of surface elements
N_{cav} = number of surface elements over cavity
N_{wet} = number of surface elements over wetted surface, $N_{wet} + N_{cav} = N$
p_∞ = ambient pressure
p_c = cavity pressure
p = local pressure
p_k = pressure at kth control point
q = local flow speed
q_k = flow speed at kth control point
Q = local flow speed
r = radial coordinate
$\vec{r}$ = position vector, $\vec{r} = x\vec{i} + y\vec{j}$
$\vec{r}_k$ = position vector for kth control point
s = arc length
$\vec{t}$ = tangent vector
t_x, t_y = cartesian components of tangent vector
$\vec{t}_k$ = tangent vector for kth surface element
t_{x_k}, t_{y_k} = cartesian components of tangent vector for kth surface element
u,v = cartesian components of disturbance velocity
$\vec{U}_\infty$ = freestream velocity
$\vec{V}$ = disturbance velocity
VOL = cavity volume
V_{kl}^N = normal velocity influence coefficient
V_{kl}^{T-} = internal tangent velocity influence coefficient
x,y = cartesian coordinates
x_{cp_i}, y_{cp_i} = cartesian coordinates of ith control point
α = angle of attack
γ = vortex density
γ_k = vortex density on kth surface element
Γ = circulation
$\Theta(x,y)$ = $\arctan(y/x)$
ξ,η = cartesian coordinates
$\{\xi_i,\eta_i\}$ = sequence defining surface elements
ρ = fluid density
ρ_{LE} = leading edge radius
σ = cavitation number, $\sigma = \dfrac{p_\infty - p_c}{\frac{1}{2}\rho U_\infty^2}$
ϕ = disturbance velocity potential
$\tilde{\phi}$ = interior velocity potential
Φ = velocity potential
ψ = disturbance stream function
Ψ = stream function

Superscripts

$-$ = interior
$+$ = exterior

Subscripts

A = at point A
B = at point B
c = cavity
cp = control point
fw = fully wetted
ℓ = at cavity termination
s = at cavity detachment
x = x-component
y = y-component

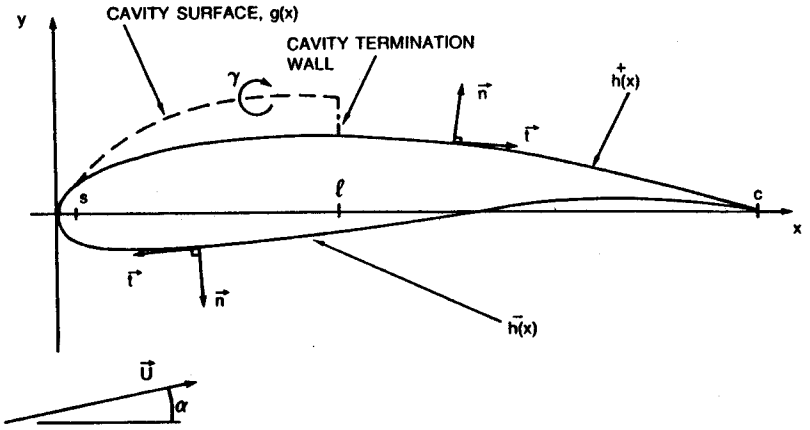

Fig. 1 Partially cavitating hydrofoil

$$\phi = \frac{-1}{2\pi}\int_C \gamma(s)\arctan\left[\frac{y-\eta(s)}{x-\xi(s)}\right]ds \tag{4}$$

Here s represents arc length about the foil-cavity contour, C, and $\xi(s)$ and $\eta(s)$ are the cartesian coordinates of the foil-cavity boundary parameterized on arc length. It follows that the disturbance velocity

$$\vec{V} = \nabla\phi \tag{5}$$

can be expressed as

$$\vec{V} = \frac{1}{2\pi}\oint_C \gamma(s)\left\{\vec{i}\,\frac{(y-\eta)}{(x-\xi)^2+(y-\eta)^2} - \vec{j}\,\frac{(x-\xi)}{(x-\xi)^2+(y-\eta)^2}\right\}ds \tag{6}$$

Boundary conditions

The kinematic condition on the foil-cavity boundary, C, is

$$\frac{\partial\Phi}{\partial n} = 0 \qquad \text{on } C \tag{7}$$

or

$$\vec{n}\cdot\vec{V} = -\vec{n}\cdot\vec{U}_\infty \qquad \text{on } C \tag{8}$$

where $\vec{n}$ is the unit outward normal vector to the boundary.

A dynamic boundary condition must also be applied on the cavity boundary. This involves Bernoulli's equation, which in dimensional terms states that

$$p_\infty + \frac{1}{2}\rho|U_\infty|^2 = p_c + \frac{1}{2}\rho Q^2 \qquad \text{on } C_c \tag{9}$$

Here p_∞ is the freestream ambient pressure, p_c is the cavity pressure (assumed uniform) and Q is the surface velocity on the cavity boundary, C_c. In nondimensional form this becomes

$$Q^2 = 1 + \sigma \qquad \text{on } C_c \tag{10}$$

where

$$\sigma = \frac{p_\infty - p_c}{\frac{1}{2}\rho U_\infty^2} \tag{11}$$

is the cavitation number and

$$Q = |\vec{U}_\infty + \vec{V}| \tag{12}$$

A Kutta condition is required at the trailing edge to uniquely specify the circulation. In its most general form it states that the flow velocity at the trailing edge (Fig. 2) remains bounded, that is

$$|\vec{V}|_{TE} < \infty \tag{13}$$

In the linear theory of cavitation a cavity closure condition is also required. In its usual form this condition states that the net flux from the foil-cavity system is zero. Since the present method uses a surface vorticity distribution, the flux is necessarily zero and a closure condition in the same vein as the linear theory is inappropriate. A cavity termination model, however, is required. The model adopted here is essentially a Riabouchinsky model in that there is no reentrant jet and no finite wake.

In purely potential-flow theory the location of the cavity detachment point would be determined by the Brillouin-Villat condition, which states that the curvature of the boundary streamline be continuous at the detachment point. In a real liquid, however, the location of the detachment point is governed by viscous effects and is generally found to be downstream of the location determined by using the Brillouin-Villat criterion (see Arakeri [40]). In light of this, the cavity detachment location has been left as an input parameter to the numerical procedure.

Alternate boundary conditions

The boundary conditions (8) and (10), given in the previous section, are exact. Together with the Kutta condition (13) and the cavity termination model these conditions yield sufficient information to determine the unknown vorticity distribution and cavity shape. There exist, however, alternate but equivalent formulations of these boundary conditions which are better suited to a numerical solution. The reasons for this will be discussed later in the section on numerical formulation; only the mathematical formulations are given here.

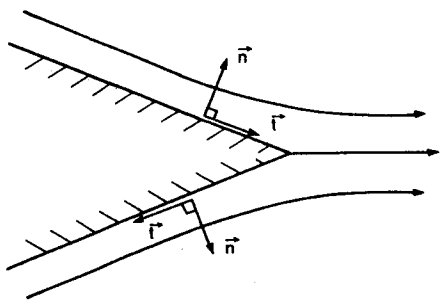

Fig. 2 Local trailing-edge flow for partially cavitating hydrofoil

An alternate form of the kinematic boundary condition is

$$\vec{t} \cdot \vec{V}^- = -\vec{t} \cdot \vec{U} \qquad \text{on } C \tag{14}$$

where $\vec{V}^-$ denotes the disturbance velocity on the interior of the foil-cavity boundary. To show this, one notes that this condition is equivalent to stating that

$$\frac{\partial \Phi^-}{\partial t} = 0 \qquad \text{on } C \tag{15}$$

where again the superscript denotes the interior. However, this condition means that Φ is a constant on the interior of the foil-cavity boundary, and the maximum principle for potential functions then states that Φ is constant on the entire interior region. With this fact it is evident that

$$\frac{\partial \Phi^-}{\partial n} = 0 \qquad \text{on } C \tag{16}$$

but since normal velocities are continuous across vortex sheets (see Appendix) one finds that

$$\frac{\partial \Phi^+}{\partial n} = 0 \qquad \text{on } C \tag{17}$$

where the superscript denotes the exterior of the foil-cavity boundary. The original boundary condition has thus been recovered.

Another form of the kinematic boundary condition is useful on the cavity surface. If

$$\vec{n} = n_x \vec{i} + n_y \vec{j} \tag{18}$$

and

$$\vec{V} = u\vec{i} + v\vec{j} \tag{19}$$

then equation (8) may be written as

$$n_x[u + \cos(\alpha)] = -n_y[v + \sin(\alpha)] \tag{20}$$

Denoting the shape of the cavity by $g(x)$, then on the cavity surface one finds

$$\frac{dg}{dx} = \frac{-n_x}{n_y} \tag{21}$$

Hence the kinematic boundary may be condition written as

$$\frac{dg}{dx} = \frac{v + \sin(\alpha)}{u + \cos(\alpha)} \tag{22}$$

The dynamic boundary condition also has alternate formulations. One way of writing this boundary condition is

$$[\vec{t} \cdot (\vec{U}_\infty + \vec{V})]^2 + [\vec{n} \cdot (\vec{U}_\infty + \vec{V})]^2 = (1 + \sigma) \qquad \text{on } C_c \tag{23}$$

Since the kinematic boundary condition is also applied on the cavity boundary, the above simplifies to

$$[\vec{t} \cdot (\vec{U}_\infty + \vec{V})]^2 = (1 + \sigma) \qquad \text{on } C_c \tag{24}$$

This equation is still nonlinear. However, one usually knows the direction of flow along the cavity, so if one selects $\vec{t}$ in such a manner that

$$\vec{t} \cdot (\vec{U}_\infty + \vec{V}) > 0 \qquad \text{on } C_c \tag{25}$$

then the square root of equation (24) may be taken. Keeping this in mind and being forwarned that in the numerical procedure it is more convenient to set the cavity length and solve for the cavitation number, instead of vice versa, the dynamic boundary condition becomes

$$\vec{t} \cdot \vec{V} - \sqrt{(1 + \sigma)} = -\vec{t} \cdot \vec{U}_\infty \tag{26}$$

One now has an equation that is exact and yet linear in the quantities $\vec{t} \cdot \vec{V}$ and $\sqrt{(1 + \sigma)}$.

Since the procedure used involves a surface vorticity distribution, there is yet another way to formulate the dynamic boundary condition. The alternate kinematic boundary condition stated that

$$\vec{t} \cdot (\vec{U}_\infty + \vec{V}^-) = 0$$

Using this and the fact that the jump in tangential velocities across a vortex sheet is equal to the local vortex strength, that is

$$\gamma = \vec{t} \cdot (\vec{U}_\infty + \vec{V}^+) - \vec{t} \cdot (\vec{U}_\infty + \vec{V}^-) \tag{27}$$

one may replace the surface velocity in equation (24) by γ, and take the square root to arrive at the dynamic boundary condition

$$\gamma - \sqrt{(1 + \sigma)} = 0 \tag{28}$$

One must exercise great care when using these dynamic boundary conditions obtained by taking the square root of Bernoulli's equation. The definitions of positive vorticity and of the tangent vector must be carefully considered or the assumption of taking the positive root of both sides may be invalid.

The Kutta condition can also be expressed in alternate forms. If one restricts one's attention to hydrofoils with finite trailing-edge angles, then in the partially cavitating case the local flow at the trailing edge must resemble the flow about a wedge (see Fig. 2). For the Kutta condition to be satisfied the flow must possess a stagnation point at the trailing edge. In this case the flow will be symmetric top and bottom and thus an equivalent statement of the Kutta condition is

$$\vec{t}_A \cdot (\vec{U}_\infty + \vec{V}_A) = -\vec{t}_B \cdot (\vec{U}_\infty + \vec{V}_B) \tag{29}$$

where A and B refer to points on the upper and lower surfaces, respectively, which are equidistant from the trailing edge. The flow about a partially cavitating hydrofoil resembles a wedge flow only in the region very close to the trailing edge, however, and hence the symmetry condition (29) holds only as A and B approach the trailing edge. Thus for a partially cavitating hydrofoil the symmetry condition must be that

$$\lim_{A \to TE} \vec{t}_A \cdot (\vec{U}_\infty + \vec{V}_A) = -\lim_{B \to TE} \vec{t}_B \cdot (\vec{U}_\infty + \vec{V}_B) \tag{30}$$

Other quantities of interest

The cavity volume (or more precisely, the sectional area) is of great interest. In an unsteady case the volume velocity determines the monopole-type acoustic source strength. If one is given to quasi-steady analysis, then the difference between the maximum and minimum cavity volume is directly proportional to the volume velocity. If $g(x)$ denotes the cavity shape, as before, and $h^+(x)$ denotes the upper surface of the hydrofoil, then the cavity volume is simply

$$\text{VOL} = \int_s^\ell [g(x) - h^+(x)]dx \tag{31}$$

where s is the cavity detachment point and ℓ is the cavity length.

The lift is also of interest. The lift coefficient is given by

$$C_L = 2\Gamma \tag{32}$$

where Γ is the non-dimensional circulation about the foil-cavity system. It is given by

$$\Gamma = \oint_C (\vec{U}_\infty + \vec{V}) \cdot d\vec{s} \tag{33}$$

The contour C is some contour that surrounds the hydrofoil-cavity system. In potential flow the above integral is path invariant as long as the path remains in the fluid. Thus one may deform the contour C until it coincides with the foil-cavity

boundary. At this point the integrand becomes known and one can rewrite equation (33) as

$$\Gamma = \oint_C (\vec{U}_\infty + \vec{V}) \cdot \vec{t}\, ds \tag{34}$$

or

$$\Gamma = \oint_C \gamma(s) ds \tag{35}$$

Since the technique to be followed is a surface vorticity technique, this last expression is the most convenient; so finally

$$C_L = 2 \oint_C \gamma(s) ds \tag{36}$$

Alternatively, the lift, as well as the moment and drag, coefficients can be arrived at by suitable integrals of the pressure over the hydrofoil surface. If one defines the unit tangent vector to the surface as

$$\vec{t} = n_y \vec{i} - n_x \vec{j} \tag{37}$$

where n_x and n_y are the x and y components of the unit normal vector, then the force normal to the free stream on an element of the hydrofoil surface of length ds is

$$dL = -p\, \vec{t} \cdot \vec{U}_\infty ds \tag{38}$$

where p is the local pressure (see Fig. 3).

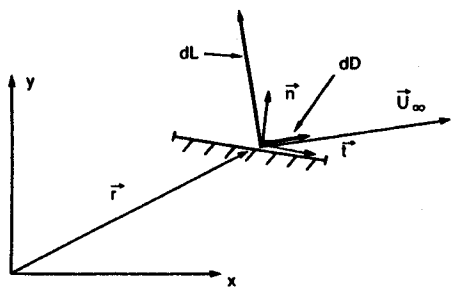

Fig. 3 Forces on a surface element

The total lift force is then

$$L = -\oint_{C_B} p\, \vec{t} \cdot \vec{U}_\infty ds \tag{39}$$

This integral must be taken along the hydrofoil boundary, C_B, not the foil-cavity boundary. In nondimensional form this becomes

$$C_L = \oint_{C_B} C_p\, \vec{t} \cdot \vec{U}_\infty ds \tag{40}$$

where

$$C_p = \frac{1}{2} \frac{p_\infty - p}{\rho U_\infty^2} \tag{41}$$

is the pressure coefficient.

Similarly the force parallel to the free stream on a surface element of length ds is

$$dD = -p\vec{n} \cdot \vec{U}_\infty ds \tag{42}$$

Thus the total drag coefficient is given by

$$C_D = \oint_{C_B} C_p \vec{n} \cdot \vec{U}_\infty ds \tag{43}$$

The moment about the origin generated by the same infinitesimal surface element is

$$dM = -p\, \vec{r} \times \vec{n}\, ds \tag{44}$$

hence the moment coefficient becomes

$$C_M = \oint_{C_B} C_p\, \vec{r} \times \vec{n}\, ds \tag{45}$$

Numerical boundary-value problem

As described in equation (6) the disturbance velocity field in the ideal fluid flow about a cavitating hydrofoil can be expressed as the integral of a surface vorticity distribution about the foil-cavity boundary. In a manner akin to Hess [31], it can be shown (see Uhlman [62]) that to lowest order in surface element length, this integral can be written as the sum of straight-line elements of constant vorticity. This representation is exact in the sense that as the number of elements increases without bound and the maximum element size approaches zero, the original integral is recovered in the limit.

The above-mentioned sum may be written as

$$\vec{V}(x,y) = \sum_{k=1}^{N} \gamma_k \{ \vec{i}\, u(x,y,\xi_{k+1},\eta_{k+1},\xi_k,\eta_k) + \vec{j}\, v(x,y,\xi_{k+1},\eta_{k+1},\xi_k,\eta_k) \} \tag{46}$$

Here γ_k is the vortex density of the kth surface element whose end points are (ξ_k,η_k) and (ξ_{k+1},η_{k+1}). The expression in brackets represents the velocity that would be induced by the kth element at the field point (x,y) if its vortex density were unity. Exact expressions are easily obtainable for u and v [62]. Note that equation (46) is linear in the γ_k's.

With equation (46) describing the velocity field, the questions of how to formulate and implement the boundary conditions must be addressed. Again following Hess, control points (x_{cp_i},y_{cp_i}) are defined by

$$\begin{aligned} x_{cp_i} &= \tfrac{1}{2}(\xi_{i+1} + \xi_i) \qquad i = 1, \ldots, N \\ y_{cp_i} &= \tfrac{1}{2}(\eta_{i+1} + \eta_i) \qquad i = 1, \ldots, N \end{aligned} \tag{47}$$

It is at these control points that the boundary conditions will be satisfied.

Since there are N control points and the kinematic boundary conditions must be satisfied at each of them for the solution to be exact, and since there are N_{cav} control points over the cavity at which the dynamic boundary condition must also be satisfied, one finds oneself with $N + N_{cav}$ equations. With the addition of the Kutta condition, the total number of equations becomes $N + N_{cav} + 1$. Having set the cavity separation location, s, and the cavity length, ℓ, the cavitation number, σ, becomes an unknown. Thus between the γ_k's and σ, the number of unknowns reaches $N + 1$. Obviously the remaining unknowns are the ordinates of the cavity shape of which there are N_{cav}.

Unfortunately, there appears to be no way to solve for all the unknowns directly and still have a linear system of equations. Due to this fact, an iterative scheme is necessary to satisfy all the boundary conditions.

The iterative scheme consists of assuming a cavity shape and satisfying only the dynamic boundary condition at the control points on the cavity. This yields N_{cav} equations. At the control points on the wetted portions of the hydrofoil, the kinematic boundary condition is satisfied, yielding N_{wet} additional equations, where $N_{wet} = N - N_{cav}$. With the addition of the Kutta condition the total number of equations reaches $N_{cav} + N_{wet} + 1$, or $N + 1$ total equations. Since the γ_k's and σ yield a total of $N + 1$ unknowns, a linear system of $N + 1$ equations in $N + 1$

unknowns is obtained. This system of equations is then solved and the solution is used in conjunction with the kinematic boundary condition over the cavity to generate a new cavity shape. This iteration procedure is then repeated until convergence is obtained, at which point all the boundary conditions are satisfied exactly.

The cavity termination model must be considered when the kinematic boundary condition is invoked to generate a new cavity shape. The numerical equivalent of equation (22) is integrated back from the leading edge of the cavity with the initial condition that the leading edge of the cavity remain on the foil. If one proceeds in this manner, one finds that the cavity trailing edge does not end on the foil. Hence to close the foil-cavity boundary contour, a cavity termination "wall" is fashioned which connects the trailing edge of the cavity to the foil (see Fig. 4). The surface elements forming this wall are treated as part of the wetted portion of the hydrofoil.

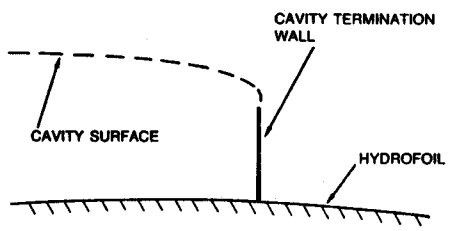

Fig. 4 Riabouchinsky-type cavity termination model

As mentioned before, the reentrant jet model is the most physically realistic cavity termination model in the sense that the streamlines of the actual fluid flow are best represented. The next most realistic cavity termination model is the Riabouchinsky type. The two models have many similarities. Tulin [10] has shown, for example, that to first order, both models require cavity closure in the linearized theory. The most salient point, however, may be that both models have a stagnation point on the hydrofoil at the aft end of the cavity. This stagnation point has been found experimentally by Meijer [41]. Hence in order to imitate physical reality as best as possible, a cavity termination model with this feature should be chosen. Other cavity termination models have also been studied, for example, Wu's open-wake model. None of the other models, however, have a stagnation point at the after end of the cavity.

The cavity termination model employed in the present work is of the modified Riabouchinsky type. The classic Riabouchinsky model applies only to supercavitating flow in that it "closes" the two free streamlines bounding the cavity with an image body downstream. This closure is done in such a manner that the circulation about the body-cavity-image system is zero. This classic form has no analog in partially cavitating flow because the Kutta condition at the trailing edge of the hydrofoil determines the circulation, which in general will be nonzero. Instead, a modified form of the Riabouchinsky cavity termination model is used. In this modified form, the cavity is closed with a short vertical "wall" on which the kinematic boundary condition is satisfied. Hence, at the juncture between the wall and the hydrofoil, a concave corner flow is established. This corner flow yields the aforementioned stagnation point (Fig. 5).

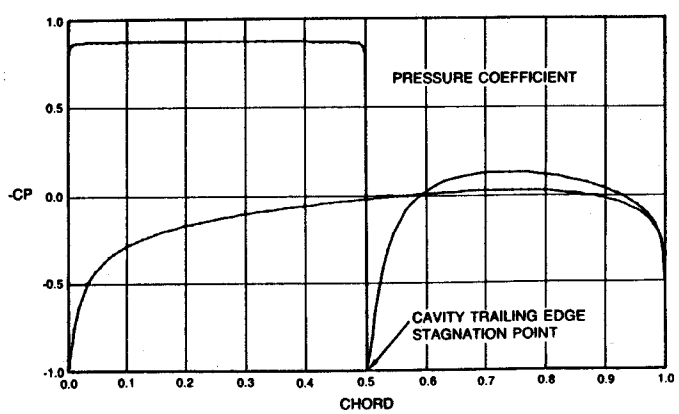

Fig. 5 NACA 16-006 section pressure distribution $\alpha = 4$ deg, $\ell/c = 0.50$

Having described the general nature of the iterative procedure, the explicit form of the boundary conditions in the numerical formulation can now be described. The kinematic boundary condition as expressed in equation (8)

$$\vec{n} \cdot \vec{V} = -\vec{n} \cdot \vec{U}_\infty \tag{48}$$

where $\vec{V}$ is the disturbance velocity field and $\vec{U}_\infty = \cos(\alpha)\vec{i} + \sin(\alpha)\vec{j}$ is the free-stream, can easily be expressed in numerical form. If one defines

$$V_{ki}^N = n_{x_i} \cdot u(x_{cp_i}, y_{cp_i}, \xi_{k+1}, \eta_{k+1}, \xi_k, \eta_k) + n_{y_i} \cdot v(x_{cp_i}, y_{cp_i}, \xi_{k+1}, \eta_{k+1}, \eta_{k+1}, \xi_k, \eta_k) \tag{49}$$

then V_{ki}^N is the normal velocity that the kth surface element would induce at the ith control point if the vortex density of the kth surface element were unity. With this convention, equation (48) may be written in discrete form as

$$\sum_{k=1}^{N} \gamma_k V_{ki}^N = -[n_{x_i} \cos(\alpha) + n_{y_i} \sin(\alpha)] \tag{50}$$

However, this form of the kinematic boundary condition is not used. This is due to the fact that a constant distribution of vorticity on a straight-line segment will induce no normal velocity at the midpoint of that segment; therefore, all the influence coefficients of the form V_{ii}^N will be zero. Thus, the main diagonal of the matrix formed, in part, from equation (50) will contain zeros and the matrix will be ill-conditioned. In order to circumvent this problem, one must use an alternate form of the kinematic boundary condition, such as that given in equation (14)

$$\vec{t} \cdot \vec{V} = -\vec{t} \cdot \vec{U}_\infty \tag{51}$$

Expressed in discrete form this equation becomes

$$\sum_{k=1}^{N} \gamma_k V_{ki}^{T-} = -[t_{x_i} \cos(\alpha) + t_{y_i} \sin(\alpha)] \tag{52}$$

where

$$V_{ki}^{T-} = t_{x_i} \cdot u^-(x_{cp_i}, y_{cp_i}, \xi_{k+1}, \eta_{k+1}, \xi_k, \eta_k) + t_{y_i} \cdot v^-(x_{cp_i}, y_{cp_i}, \xi_{k+1}, \eta_{k+1}, \xi_k, \eta_k).] \tag{53}$$

The superscript "$-$" denotes that all velocities are to be calculated on the interior of the foil-cavity boundary. Thus V_{ki}^{T-} represents the internal tangent velocity induced at the ith control point by the kth surface element if the vortex density of the kth surface element were unity. In this formulation, the influence coefficients of the form V_{ii}^{T-} have the largest absolute value, so the matrix in question becomes diagonally dominant and therefore better conditioned. This is the form of the kinematic condition that is employed during each iteration cycle when solving for the unknown σ and γ_k's.

The dynamic boundary condition can be expressed numerically in two ways. Referring to equation (26), that is

$$\vec{t} \cdot \vec{V} - \sqrt{(1+\sigma)} = -\vec{t} \cdot \vec{U}_\infty \tag{54}$$

one may express the dynamic boundary condition in the form

$$\sum_{k+1}^{N} \gamma_k V_{kt}^{T+} - \sqrt{(1+\sigma)} = -(t_{x_i} \cos(\alpha) + t_{y_i} \sin(\alpha)) \tag{55}$$

Here the superscript "+" denotes the fact that the induced velocities are to be calculated on the exterior of the foil-cavity boundary. It should also be noted that one is not solving for σ directly, rather the quantity $\sqrt{(1+\sigma)}$ is being considered an unknown from which σ can be derived at a later time.

Another form for the dynamic boundary condition is

$$\gamma - \sqrt{(1+\sigma)} = 0 \tag{56}$$

as given in equation (28). Expressed numerically this becomes simply

$$\gamma_i - \sqrt{(1+\sigma)} = 0 \tag{57}$$

Either form of the dynamic boundary condition can be used. In practice it has been found that the fastest and most stable convergence is achieved by averaging the two alternate forms. Hence, all results presented herein have been arrived at in this manner.

Equation (30) is referred to in order to formulate the numerical Kutta condition. This equation states that the surface velocities on the upper and lower surfaces of the hydrofoil must be equal at the trailing edge. Since in the present formulation there is no control point at the trailing edge, the surface velocities on the upper and lower surfaces at the trailing edge are obtained by linear extrapolation from the surface velocities at the two control points adjacent to the trailing edge on each surface. Thus, if a_1 denotes the arc length from the trailing edge of the hydrofoil to the first control point on the upper surface, and if a_2 denotes the arc length from the trailing edge to the second control point on the upper surface, then the surface velocity at the trailing edge on the upper surface is approximated by

$$q_{TE}^{upper} = \frac{q_1 a_2 - q_2 a_1}{a_2 - a_1} \tag{58}$$

Here, q_1 and q_2 are the surface velocities at the first and second control points respectively, that is

$$q_1 = \sum_{k=1}^{N} \gamma_k V_{k1}^{T+} + \vec{t}_1 \cdot \vec{U}_\infty$$

and (59)

$$q_2 = \sum_{k=1}^{N} \gamma_k V_{k2}^{T+} + \vec{t}_2 \cdot \vec{U}_\infty$$

Since the two control points on the lower surface adjacent to the trailing edge of the hydrofoil are the Nth and $(N-1)$th, one may similarly define a_N and a_{N-1} as the appropriate arc lengths from the trailing edge, and q_N and q_{N-1} as the corresponding surface velocities

$$q_N = \sum_{k=1}^{N} \gamma_k V_{kN}^{T+} + \vec{t}_N \cdot \vec{U}_\infty$$

(60)

$$q_{N-1} = \sum_{k=1}^{N} \gamma_k V_{k(N-1)}^{T+} + \vec{t}_{N-1} \cdot \vec{U}_\infty$$

With these quantities defined, one may write the extrapolated surface velocity at the trailing edge on the lower surface velocity as

$$q_{TE}^{lower} = \frac{q_N a_{N-1} - q_{N-1} a_N}{a_{N-1} - a_N} \tag{61}$$

Using equations (58), (59), (60) and (61), and bearing in mind that the tangent vectors differ in direction on the upper and lower surfaces, one may write the Kutta condition as

$$\sum_{k-1}^{N} \gamma_k \left\{ \frac{a_2 V_{k1}^{T+} - a_1 V_{2k}^{T+}}{a_2 - a_1} + \frac{a_{N-1} V_{kN}^{T+} - a_N V_{k(N-1)}^{T+}}{a_{N-1} - a_N} \right\}$$

$$= -\vec{U}_\infty \cdot \left\{ \frac{a_2 \vec{t}_1 - a_1 \vec{t}_2}{a_2 - a_1} + \frac{a_{N-1} \vec{t}_N + a_N \vec{t}_{N-1}}{a_{N-1} - a_N} \right\} \tag{62}$$

The numerical formulation of the boundary conditions and Kutta condition necessary to form the matrix which is solved for the γ_k's and σ at each iteration is now complete. The matrix is formed from the following equations:

KINEMATIC BOUNDARY CONDITIONS

$$\sum_{k=1}^{N} \gamma_k V_{kt}^{T-} = -\vec{t}_i \cdot \vec{U}_\infty, \qquad i = 1, \ldots, N_{wet} \tag{63}$$

DYNAMIC BOUNDARY CONDITIONS

$$\sum_{k=1}^{N} \gamma_k V_{kt}^{T+} - \sqrt{(1+\sigma)} = -\vec{t}_i \cdot \vec{U}_\infty,$$

$$i = N_{wet} + 1, \ldots, N_{wet} + N_{cav} \tag{64}$$

and the Kutta condition as given in equation (62). These equations are then solved using Gaussian elimination with partial pivoting.

At this point, the dynamic boundary condition is satisfied on an assumed cavity surface and the kinematic boundary condition is satisfied on the wetted portions of the hydrofoil. The kinematic boundary condition is not, however, satisfied on the cavity unless the correct cavity location has been determined. The essence of the iteration procedure is to determine the correct cavity location. To do so, the solution determined above is used in conjunction with the kinematic boundary condition as expressed in equation (22), that is

$$\frac{dg}{dx} = \frac{\sin(\alpha) + v}{\cos(\alpha) + u} \tag{65}$$

The assumption is made that the cavity leading edge remains attached to the hydrofoil and equation (65) is then integrated from the leading edge to the trailing edge of the cavity. Once the ordinate of the trailing edge of the cavity is known, surface elements are erected to form the Riabouchinsky wall connecting the trailing edge of the cavity to the hydrofoil. Numerically, equation (65) is expressed as

$$\frac{g_{i+1} - g_i}{x_{i+1} - x_i} = \frac{\sin(\alpha) + \sum_{k=1}^{N} \gamma_k V_{kt}}{\cos(\alpha) + \sum_{k=1}^{N} \gamma_k U_{kt}} \tag{66}$$

where (x_i, g_i) are the coordinates of the end points of the surface elements on the cavity and (U_{kt}, V_{kt}) denotes the cartesian velocity induced at the ith control point, (x_{cp_i}, y_{cp_i}), by the kth surface element assuming its vortex density is one. Assuming for the moment that the index i begins at the leading edge of the cavity and increases toward the trailing edge of the cavity, equation (66) may be written in the form of a recursion relation defining the new cavity ordinates as

$$g_{i+1} = g_i + (x_{i+1} - x_i)\frac{\sin(\alpha) + \sum_{k=1}^{N} \gamma_k V_{ki}}{\cos(\alpha) + \sum_{k=1}^{N} \gamma_k U_{ki}}, \qquad i = 1, \ldots, N_{cav} \tag{67}$$

With the new cavity location determined, the Riabouchinsky wall is erected by simply dividing the vertical distance between the ordinate of the trailing edge of the cavity and the ordinate of the hydrofoil surface immediately below it into the surface elements allotted specifically for this purpose (see Fig. 6).

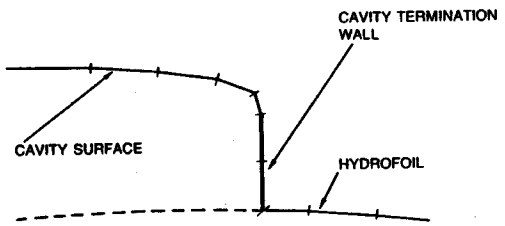

Fig. 6 Riabouchinsky cavity termination "wall"—discrete form

The unit normal and tangential vectors and the location of the control points on the Riabouchinsky wall and the new cavity surface are then redefined, and equations (62), (63) and (64) are used to form a new boundary-condition matrix which is then solved to yield the solution corresponding to the new cavity shape. This procedure is repeated until the solution has converged.

Quantities of interest

To each iteration there corresponds a cavity shape and the solution of the boundary-value problem associated with it. From these one may derive such quantities as cavity volume, lift coefficient, and moment coefficient.

To get the cavity volume, equation (31) must be expressed in numerical form. This equation may also be written as

$$\mathrm{VOL} = \int_s^\ell g(x)dx - \int_s^\ell h^+(x)dx \tag{68}$$

The last integral on the right-hand side is merely the area of the hydrofoil above the x-axis under the cavity. This quantity will not change from iteration to iteration since the cavity length is an input. The first integral on the right-hand side is the area under the cavity above the x-axis and may change from iteration to iteration. However, the first assumed cavity shape, in iteration zero, is the shape of the hydrofoil in way of the cavity; hence one may write

$$A = \int_s^\ell h^+(x)dx = \int_s^\ell g(x)dx\big|_{\mathrm{ITER}=0} \tag{69}$$

Using the same notation used in equation (67) one may express equation (68) numerically as

$$\mathrm{VOL}\big|_{\mathrm{ITER}=j} = \frac{1}{2}\sum_{k=1}^{N_{cav}} (g_{i+1} + g_i)(x_{i+1} - x_i)\big|_{\mathrm{ITER}=j} - A, \tag{70}$$

The circulation is also easy to find. By equation (35) the circulation, Γ, is just the integral of the surface vorticity about the foil-cavity boundary. In discrete form this becomes

$$\Gamma = \sum_{k=1}^{N} \gamma_k[\xi_{k+1} - \xi_k)^2 + (\eta_{k+1} - \eta_k)^2]^{1/2} \tag{71}$$

The lift coefficient, C_L, can now be found as simply twice the circulation.

An alternate method for determining the lift coefficient is given in equation (40). In discrete form this equation may be written as

$$C_L = \sum_{k=1}^{N} p_k \ell_k \vec{t}_k \cdot \vec{U}_\infty \tag{72}$$

where

$$p_k = \gamma_k^2 - 1 \tag{73}$$

is the pressure coefficient at the kth control point, ℓ_k is the length of the kth surface element on the hydrofoil, that is

$$\ell_k = [(\xi_{k+1} - \xi_k)^2 + (\eta_{k+1} - \eta_k)^2]^{1/2}\big|_{\mathrm{ITER}=0} \tag{74}$$

and

$$\vec{t}_k = n_{y_k}\vec{i} - n_{x_k}\vec{j}\big|_{\mathrm{ITER}=0} \tag{75}$$

is the unit tangent vector on the kth surface element on the hydrofoil. The notation "ITER=0" above, means that both ℓ_k and $\vec{t}_k$, as used in equation (72), refer to the element lengths and tangent vectors on the actual hydrofoil surface, not on the cavity surface. Since the hydrofoil surface and assumed cavity surface coincide at iteration zero, the values of ℓ_k and $\vec{t}_k$ for that iteration are saved and used for the evaluation of the forces in all subsequent iterations. Also, since the pressure is assumed constant in the cavity, the pressures calculated via equation (73) in way of the cavity are valid on the cavity surface as well as on the underlying hydrofoil surface and hence may be transferred directly.

Similarly, referring to equations (43) and (45), the drag and moment coefficients may also be calculated by appropriate integrals over the hydrofoil surface. Using the notation defined in equations (73), (74) and (75), these coefficients are calculated numerically as

$$C_D = \sum_{k=1}^{N} p_k \ell_k \vec{n}_k \cdot \vec{U}_\infty \tag{76}$$

and

$$C_M = \sum_{k=1}^{N} p_k \ell_k \vec{r}_k \times \vec{n}_k \tag{77}$$

Here $\vec{n}_k$ is the unit normal vector for the kth element taken at iteration zero, and $\vec{r}_k$ is the position vector from the origin to the kth control point, also taken at iteration zero.

At each iteration the quantities σ, Γ, C_L, C_D, C_M and VOL are calculated. Convergence is considered to have occurred when changes in these quantities, from one iteration to the next, are sufficiently small. Usually this is taken to be less than 1 percent.

Results and conclusions

Convergence

In the previous section it was mentioned that the present numerical formulation is exact in the sense that, as the number of surface elements tends to infinity, and the size of the largest element approaches zero, the solution converges to that of the given potential-flow problem. Due to the iterative nature of the numerical solution technique, it is likely that the number of

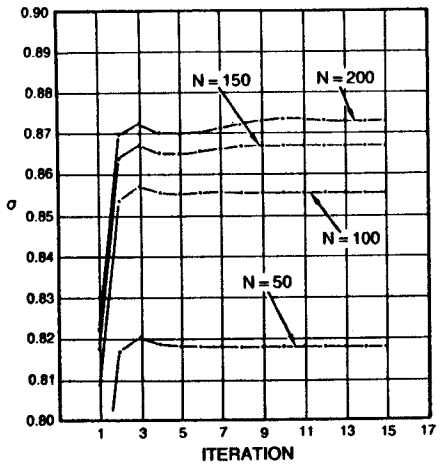

Fig. 7 Convergence, σ versus number of iterations, NACA 16-006 section, $\alpha = 4$ deg, $\ell/c = 0.50$, for $N = 50, 100, 150, 200$

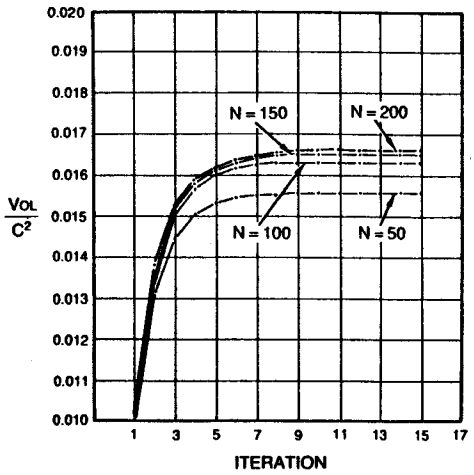

Fig. 8 Convergence, VOL/c^2 versus number of iterations, NACA 16-006 section, $\alpha = 4$ deg, $\ell/c = 0.50$, for $N = 50, 100, 150, 200$

iterations required for convergence will tend to infinity monotonically with the number of surface elements.

In order to ascertain how many surface elements and iterations are necessary to achieve reasonable convergence, a series of computations was performed. Figures 7–9 show results for an NACA 16-006 hydrofoil section at 4-deg angle of attack with a cavity length of 50 percent of the chord ($\ell/c = 0.50$). Figure 7 shows the convergence of the cavitation number, σ, as a function of the number of iterations for various numbers of surface elements. It can be seen that for all cases shown, convergence in iteration number is achieved with 15 iterations. The final difference in the cavitation number predicted, using 150 and 200 surface elements, is approximately 0.7 percent. Figure 8 shows the convergence of the cavity volume with respect to iteration number. For all cases, 15 iterations are again sufficient for convergence. The difference in predicted volume between the $N = 150$ and $N = 200$ cases is less than 0.7 percent.

These results are typical. A large number of surface elements is necessary to achieve accurate results. This is most likely due to the discrete integration scheme used to generate the cavity surface. If the discretization is not fine enough in the leading-edge region where the flow velocity is changing direction rapidly, the initial shape of the cavity will be inaccurate and, due to the integration, the entire cavity shape will be affected.

Figures 7 and 8 also indicate that the number of iterations required for convergence is a function of the number of surface elements employed. Figure 10 shows the estimated number of iterations required for convergence versus the number of surface elements. This figure was derived from the information in Fig. 7. It is easily seen that the relationship between the number of elements and the number required iterations is approximately linear. Thus to achieve convergence one must use a large number of elements and a proportional number of iterations.

The accuracy with which the boundary conditions are satisfied, at convergence, has also been investigated. This was accomplished by calculating the velocities normal and tangential to the foil-cavity boundary at the control points of the surface elements. The tangential velocities over the cavity were found to be constant to within roughly 0.05 percent of the freestream value. The normal velocities over most of the boundary were less than 0.01 percent of freestream. The only exceptions to this occurred at the leading and trailing edges of the cavity. In these regions, where the direction of the velocity changes rapidly, the normal velocities were several percent of the freestream value. This is undoubtedly due, in part, to the discrete integration scheme employed in generating the cavity shape, as the magni-

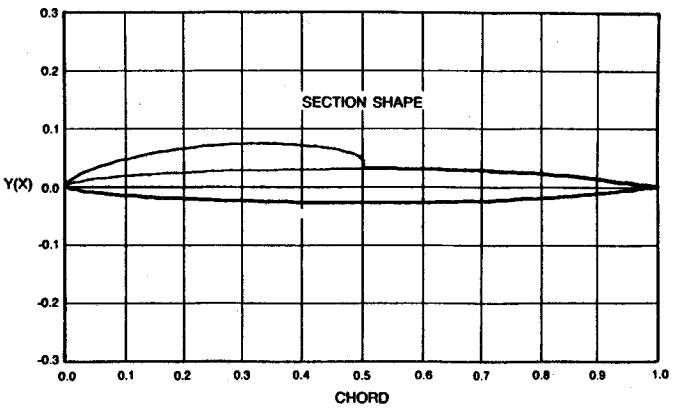

Fig. 9 Cavitating NACA 16-006 section, $\alpha = 4$ deg, $\ell/c = 0.50$, final cavity shape after 15 iterations

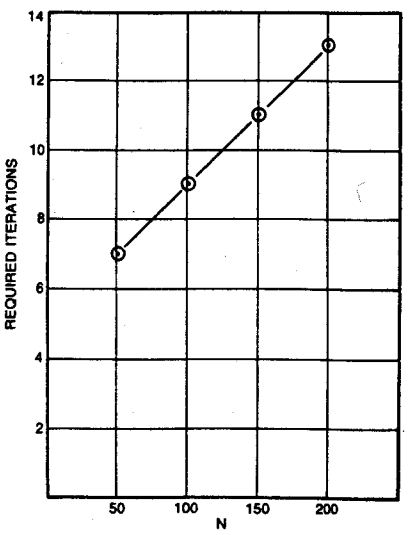

Fig. 10 Estimated number of iterations required for convergence versus number of surface elements, NACA 16-006 section, $\alpha = 4$ deg, $\ell/c = 0.50$

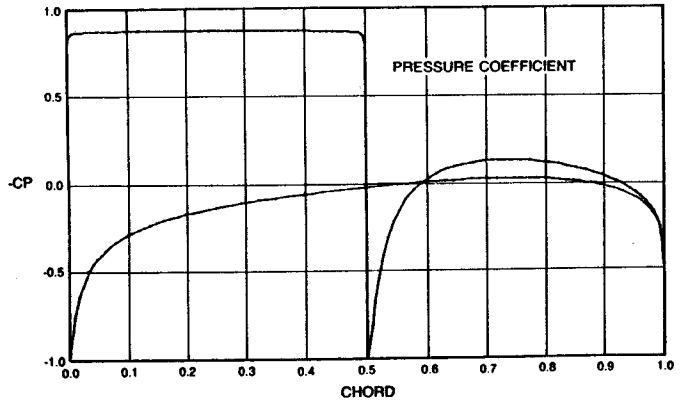

Fig. 11 Pressure distribution NACA 16-006 section, $\alpha = 4$ deg, $\ell/c = 0.50$, from PCAV

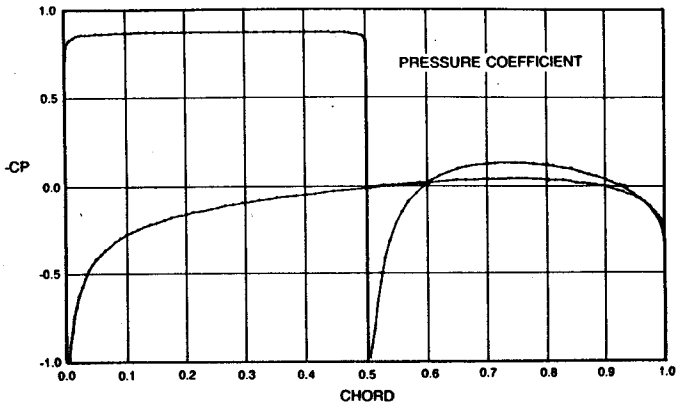

Fig. 12 Pressure distribution NACA 16 = 006 section, $\alpha = 4$ deg, $\ell/c = 0.50$, from FW

tude of these normal velocities decreases with increasing number of elements.

The accuracy of the solution was also assessed in the following manner. The output geometry from the partially cavitating hydrofoil program was employed as the input to a computer program that assumed the flow was fully wetted; that is, only the kinematic boundary condition was used. Figure 11 shows the pressure distribution over an NACA 16-006 section with a cavity length of 50 percent of the chord at an angle of attack of 4 deg. This figure was plotted using the output of the iterative partially cavitating hydrofoil program (PCAV). Figure 12 shows the pressure distribution under the same conditions, generated by the fully wetted hydrofoil program (FW) using the geometry output by PCAV after 15 iterations. These two figures are seen to be virtually identical. If the surface velocities over the cavity predicted by the fully wetted hydrofoil program are compared with those predicted by the partially cavitating hydrofoil program, the maximum error is found to be about 0.5 percent.

The effect of varying the location of the cavity detachment point was also studied. This was done by ascertaining the location of the minimum pressure point in the fully wetted condition using FW, and, on the basis of this information, altering the location of the cavity detachment point in PCAV through a reasonable range of values. The results, for an NACA 16-006 section at an angle of attack of 4 deg with a cavity whose length is 50 percent of the chord, are given in Table 1. The maximum variation in cavitation number is less than 1.0 percent, while the maximum variation in cavity volume is about 2.5 percent. If, however, one considers shorter cavity lengths or thicker foils the relative variation in these quantities can be much greater. The effect of the location of the cavity detachment point on cavitation number and cavity volume for NACA 16 series sections of 6, 9 and 12 percent thickness ratios, at 4-deg angle of attack, is given in Table 2 for a cavity length to chord ratio of 5 percent. The locations of the fully-wetted pressure minima for these sections, at this angle of attack, are 0.014, 0.112, and 0.335 percent of the chord, respectively. For the cavity volume in particular, the relative variation can be quite high, although the absolute variation is small. This is due to the small cavity volumes involved.

The effect of the location of the cavity detachment point is due to the fact that if the detachment point is set too far forward on the section, the cavity free streamline will initially pass through the locus of the hydrofoil. Thus the effect is greatest on thick foils (or more accurately, on foils with larger leading-edge radii) since a larger volume of the foil will be intersected by a cavity that begins too far forward. If the cavity detachment point is set too far aft on the hydrofoil, the pressure minimum may no longer be on the cavity surface but rather on the wetted portion of the foil upstream of the cavity.

In reality the location of the cavity detachment point will be somewhat downstream of the location of the fully wetted pressure minimum. This result was determined experimentally by Arakeri [40]. The data from Table 1 are shown graphically in Figs. 13 and 14. It can be seen that both the cavitation number and the cavity volume appear to possess maxima for a cavity detachment point located slightly downstream of the fully wetted pressure minimum. The significance of these maxima is not known.

Unfortunately, the proper location for the cavity detachment point cannot be determined a priori. Thus in view of the above results, and in consideration of a finite computer budget, all results presented subsequently have been generated using 200 surface elements and 15 iterations and with the cavity detachment point located at the position of the fully-wetted pressure minimum.

Results

In an effort to approximate as nearly as possible the exact, nonlinear, partially cavitating flow past a flat plate, computations were performed for a 1 percent thick bi-convex foil at angles of attack of 2 and 4 deg. The results are presented in Figs. 15 and 16. Upon comparison with Geurst's [21] linear theory results for a flat plate, one notes that, although the nonlinear theory predicts that the cavity length is no longer solely a function of α/σ, in general the predictions of the linear theory are

Table 1 Effect of location of cavity detachment point for NACA 16-006 section with a 50 percent cavity length

s/c	σ	C_L	C_M	VOL
0.0	0.87301	0.53500	0.12983	0.01660
0.00014	0.87513	0.53562	0.12986	0.01670
0.00088	0.87358	0.53518	0.12984	0.01660
0.00176	0.86774	0.53367	0.12979	0.01629

Table 2 Effect of location of cavity detachment point for NACA 16 series sections with 5 percent cavity lengths

	NACA 16-006 $s'/c = 0.00014$		NACA 16-009 $s'/c = 0.00112$		NACA 16-012 $s'/c = 0.00335$	
s/c	σ	VOL	σ	VOL	σ	VOL
0.0	2.07774	0.00023	1.72294	0.00011	1.37925	0.00001
s'/c	2.08881	0.00024	1.82723	0.00016	1.55850	0.00008

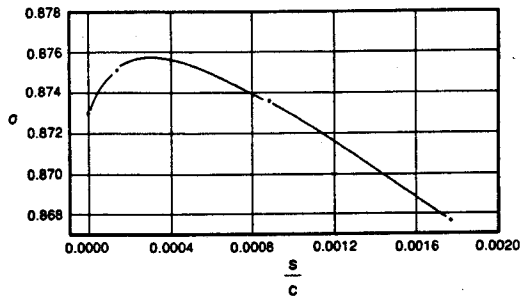

Fig. 13 σ versus s/c, NACA 16-006 section, α = 4 deg, ℓ/c = 0.50

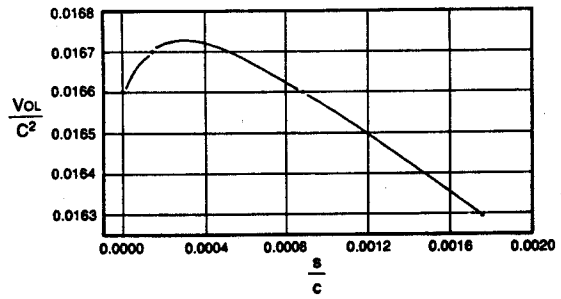

Fig. 14 VOL/c^2 versus s/c, NACA 16-006 section, α = 4 deg, ℓ/c = 0.50

good. In particular, Fig. 16 shows that, for a 1 percent thick bi-convex foil, the cavity volume predicted by nonlinear theory is linear in α. To investigate this result further, computations were made for a 4 percent bi-convex foil at angles of attack of 2 and 4 deg. Results of these computations are shown in Fig. 17, where it can be seen that for a thicker foil this linearity in α is lost.

To study the effect of hydrofoil section thickness on cavity volume, computations were made for NACA 16 sections 6, 9 and 12 percent thick at 4-deg angle of attack. Results are shown in Figs. 18 and 19. For comparison, a computer program which solves the linearized partially cavitating hydrofoil problem including thickness effects [42] was run for the same conditions. Results of this program are presented in Figs. 20 and 21.

Comparing Figures 18 and 20 one immediately notices that the effect of section thickness on cavity length in the linear theory is apparently the reverse of that in nonlinear theory. The trend of the linear theory curves for short cavities is to be expected since the presence of the leading-edge singularity in linear theory requires an infinite cavitation number to reduce the cavity length to zero. The trend of the curves generated by the nonlinear theory for short cavities is also to be expected. In this case there is no leading-edge singularity and one anticipates that the cavity length will go to zero at a finite cavitation number. The values of α/σ for ℓ/c = 0.0 in Fig. 18 were determined by using the maximum surface velocity found on the hydrofoil in the fully wetted condition to derive an inception cavitation number. It should also be mentioned that the nonlinear results exhibit the same sort of behavior for long cavity lengths as the linear theory. Namely, the cavitation number tends to increase for cavity lengths in excess of about 75 percent of chord. It has been suggested [43] that this is due to the proximity of the stagnation points at the end of the cavity and the trailing edge of the hydrofoil.

Figures 19 and 21 show the effect of section thickness on cavity volume according to nonlinear theory and linear theory, respectively. It is immediately apparent that the linear theory significantly underpredicts the magnitude of this effect. For example, for a cavity length of 50 percent of chord the nonlinear results

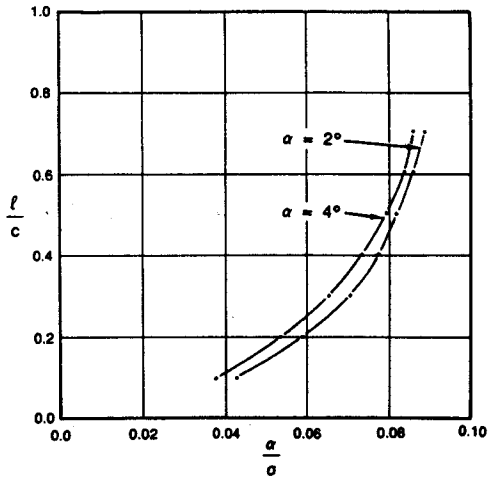

Fig. 15 ℓ/c versus α/σ, 1 percent thick bi-convex foil

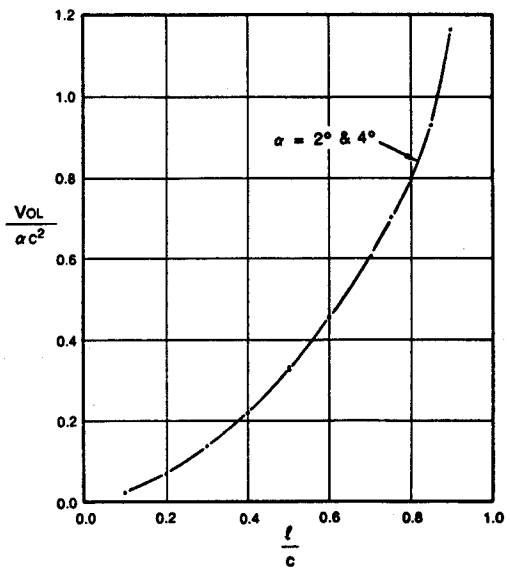

Fig. 16 VOL/αc^2 versus ℓ/c, 1 percent thick bi-convex foil

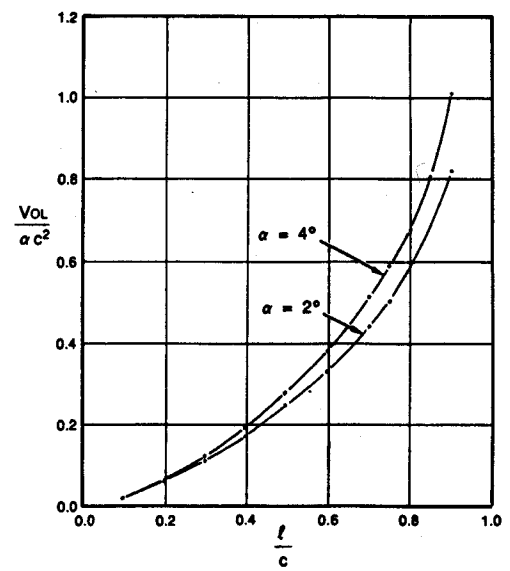

Fig. 17 VOL/αc^2 versus ℓ/c, 4 percent thick bi-convex foil

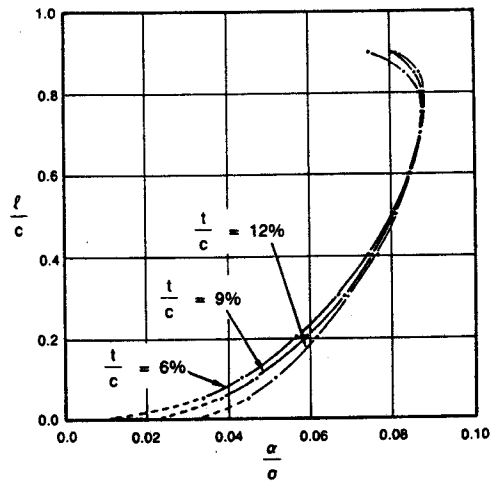

Fig. 18 ℓ/c versus α/σ, NACA 16 series sections, α = 4 deg

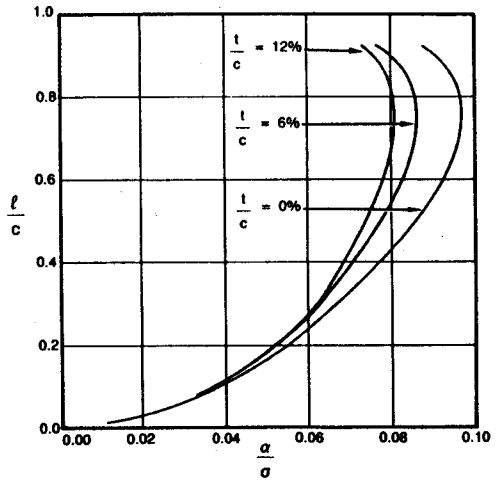

Fig. 20 ℓ/c versus α/σ, NACA 16 series sections, linear results with thickness, α = 4 deg

predict that increasing the thickness ratio from 6 to 12 percent decreases the cavity volume by over 40 percent. The linear theory, in contrast, predicts a decrease of less than 11 percent. Also, for a 6 percent thick foil with this cavity length, the nondimensional cavity volume determined by the nonlinear theory is about 0.013. The corresponding result from the linear theory is about 0.023. Thus the linear theory overpredicts this cavity volume by approximately 77 percent.

Another approach which has been put forth in an effort to predict the effect of thickness is the "short cavity" theory of Tulin and Hsu [39]. Instead of perturbing the freestream flow, as is done in conventional linear theory, Tulin and Hsu perturb an exact solution for the fully wetted flow about the hydrofoil. Results gleaned from their work [39] are presented in Fig. 22. To facilitate the comparison with their results, the data already presented in Figs. 18–21 have been reshuffled into the format used by Tulin and Hsu. Figures 23 and 24, therefore, present VOL/c^2 versus α/σ as predicted by the nonlinear theory and the linear theory with thickness, respectively.

Upon comparison of these three figures, it is readily apparent that the effect on cavity volume due to foil thickness, as indicated by the linear theory, is the opposite of the effect predicted by the other two theories. For $\alpha/\sigma \gtrsim 0.06$, the linear theory predicts that increasing the foil thickness will increase the cavity volume. Both the present nonlinear theory and the Tulin/Hsu theory, however, predict that the cavity volume will decrease as section thickness increases, regardless of the value of α/σ.

Tulin and Hsu's theory indicates a drastic effect of section thickness on cavity volume. If one examines their results for α/σ = 0.07, for example, one sees that increasing the thickness ratio from 6 to 9 percent yields a reduction in cavity volume of about 80 percent. If one increases the thickness ratio from 6 to 12

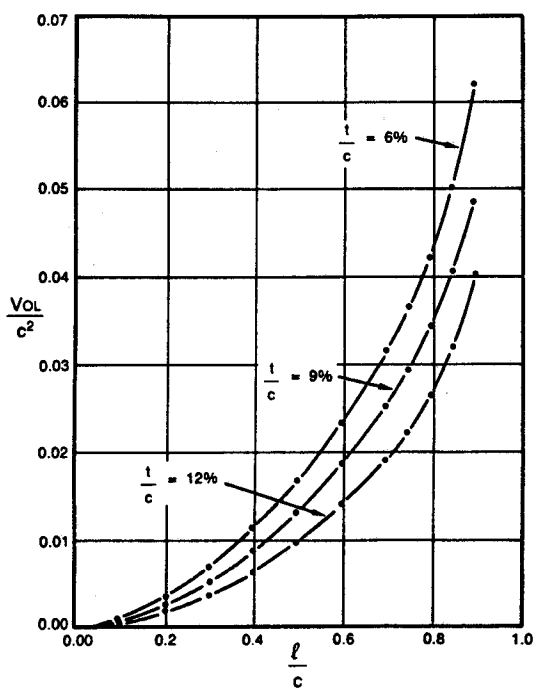

Fig. 19 VOL/c^2 versus ℓ/c, NACA 16 series sections, nonlinear results, α = 4 deg

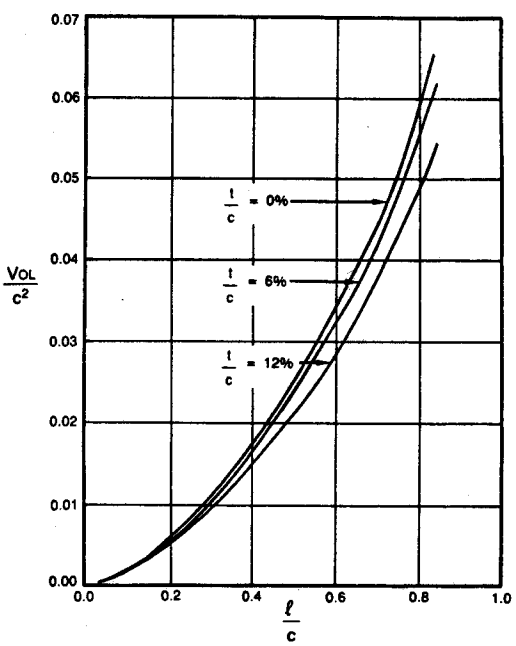

Fig. 21 VOL/c^2 versus ℓ/c, NACA 16 series sections, linear results with thickness, α = 4 deg

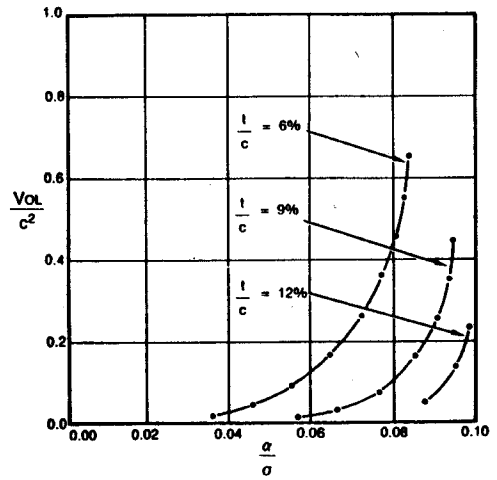

Fig. 22 VOL/c^2 versus α/σ, NACA 16 series sections, Tulin and Hsu's results, α = 4 deg

percent, the reduction in cavity volume is virtually 100 percent. The present theory is more conservative in its predictions. For α/σ = 0.07, it predicts only a 33 percent reduction in cavity volume when the section thickness ratio is raised from 6 to 9 percent. Similarly, raising the thickness ratio from 6 to 12 percent yields about a 64 percent loss of cavity volume.

In order to determine whether this "thickness effect" is truly due to section thickness or is actually due to the change in leading-edge radius with changing thickness ratio, further computations were performed. Three new hydrofoil sections were generated for these computations using an analytically defined series due to Kerwin [56] which allows the section thickness ratio and the leading-edge radius to be set independently. All three sections are 6 percent thick and their leading-edge radii are 0.176, 0.352 and 0.704 percent of the chord, respectively. These shall henceforth be referred to as Kerwin Sections A, B and C. Section A has the same thickness ratio and leading-edge radius as an NACA 16-006 section and Section C has the same leading

Table 3 Effect of leading-edge radius for a constant thickness ratio on Kerwin series sections

			α = 4 deg			
	Kerwin A		Kerwin B		Kerwin C	
	$\frac{\rho}{c}$ = 0.00176		$\frac{\rho}{c}$ = 0.00352		$\frac{\rho}{c}$ = 0.00704	
	$\frac{s'}{c}$ = 0.00014		$\frac{s'}{c}$ = 0.00124		$\frac{s'}{c}$ = 0.00359	
ℓ/c	σ	VOL	σ	VOL	σ	
VOL						
0.05	2.01461	0.00022	2.00041	0.00017	1.94714	0.00011
0.50	0.87775	0.01618	0.88969	0.01620	0.90888	0.01639

Table 4 NACA 16 series sections results for 5 and 50 percent cavity lengths

			α = 4 deg			
	NACA 16-006		NACA 16-009		NACA 16-012	
	$\frac{\rho}{c}$ = 0.00176		$\frac{\rho}{c}$ = 0.00396		$\frac{\rho}{c}$ = 0.00703	
	$\frac{s'}{c}$ = 0.00014		$\frac{s'}{c}$ = 0.00112		$\frac{s'}{c}$ = 0.00335	
ℓ/c	σ	VOL	σ	VOL	σ	
VOL						
0.05	2.08881	0.00024	1.82723	0.00016	1.55850	0.00008
0.50	0.87513	0.01670	0.86924	0.01305	0.86255	0.00954

radius as an NACA 16-012 section. Thus a comparison of the relative effects of section thickness and leading-edge radius can be made.

The computational results for the Kerwin sections with cavity lengths of 5 and 50 percent of chord are given in Table 3. Corresponding results for the NACA sections are given in Table 4. It can easily be seen that for a 5 percent cavity length the results for both series are comparable. For a cavity length of 50 percent of the chord, however, the results differ widely. In this case the results for the Kerwin sections remain fairly constant with only a slight increase in cavity volume with increasing

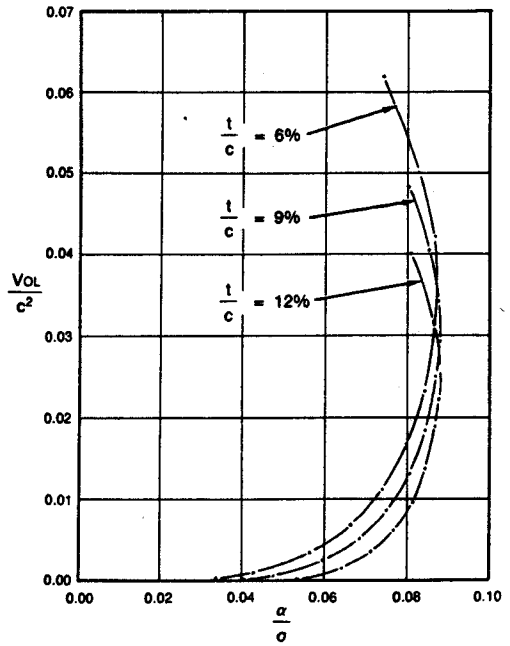

Fig. 23 VOL/c^2 versus α/σ, NACA 16 series section, α = 4 deg

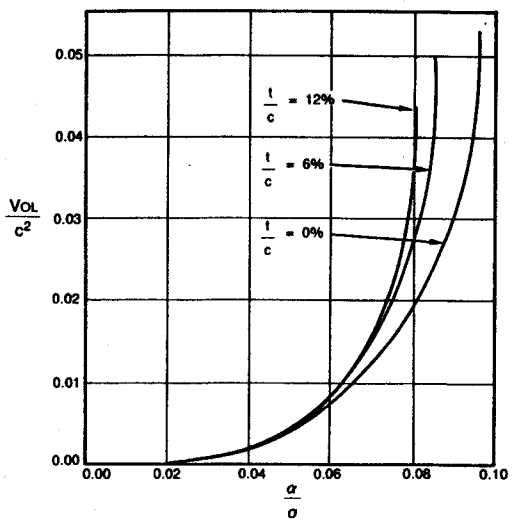

Fig. 24 VOL/c^2 versus α/σ, NACA 16 series sections, linear results with thickness, α = 4 deg

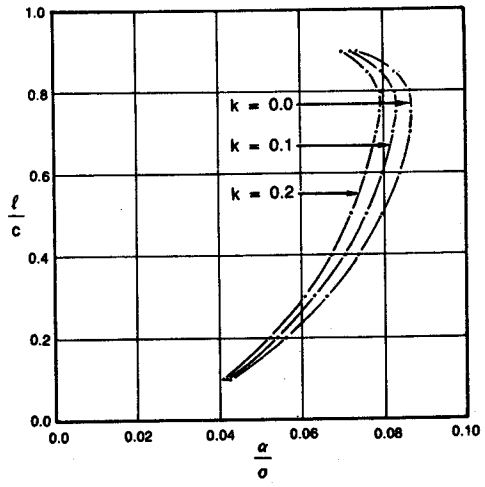

Fig. 25 ℓ/c versus α/σ, camber results, k = design lift coefficient, NACA 16-006 section and a = 0.8 meanline, α = 4 deg

leading-edge radius. The NACA 16 series sections, however, exhibit a dramatic decrease in cavity volume with increasing thickness ratio. These results indicate that short cavities are controlled by the leading-edge radius. Long cavities, that is, cavities whose length is much, much greater than a leading-edge radius, are governed by the section thickness itself and not the leading-edge radius. From a practical point of view this latter effect is the more important one, since long cavities necessarily entail greater cavity volume.

The effect of camber has also been investigated with the present nonlinear theory. In order to compare results with Tulin and Hsu, the computations were carried out for cambered foils constructed from an a = 0.8 meanline and an NACA 16-006 thickness section. Three hydrofoil sections were studied. They differed only in the amount of camber, the design lift coefficients being 0.0, 0.1 and 0.2, respectively. Results of these computations are presented in Figs. 25–27.

Figure 25 indicates that, over the primary range of interest $0.0 < \ell/c < 0.75$, an increase in camber yields an increase in cavity length. Figure 26 shows that if one holds cavity length constant, an increase in camber yields a decrease in cavity volume. If, however, the operating conditions are held constant, that is constant α/σ, increasing the camber increases cavity volume. Using the results presented in Fig. 27, for example, one finds that, for $\alpha/\sigma = 0.07$, doubling the camber from a design lift coefficient of 0.1 to a design lift coefficient of 0.2 raises the predicted cavity volume by almost 30 percent.

Corresponding results obtained by Tulin and Hsu [39] are presented in Fig. 28. Their results indicate that for $\alpha/\sigma = 0.07$ the same doubling of the camber, as discussed above, yields as increase of cavity volume of more than 70 percent.

A further comparison may be made if one considers Geurst and Verbrugh's [22] theory for a zero-thickness partially cavitating parabolic camber line. These results are shown in Fig. 29 for parabolic camber lines at 4-deg angle of attack with design lift coefficients of 0.0, 0.1 and 0.2. The increase in cavity volume achieved by doubling the design lift coefficient from 0.1 to 0.2 for $\alpha/\sigma = 0.07$ is approximately 11 percent according to this theory.

For any theory to be considered valid its results must compare favorably with experimental results. Unfortunately, for the present case, experimental data are lacking. Meijer [41] performed experiments on a 4 percent thickness ratio plano-convex section and a 4 percent thickness ratio bi-convex section. Wade and Acosta [44] studied the cavitating flow past a 7 percent thick plano-convex section. Uhlman and Jiang [45] investigated a partially cavitating plano-convex section of 6 percent thickness ratio.

Comparison of the present non-linear results, ℓ/c versus α/σ, for a 4 percent thick bi-convex foil with Meijer was unilluminating. The experimental scatter is such that, although the nonlinear results appeared slightly better, nothing definitive could be said (see Fig. 30).

The only cavitating round-nosed hydrofoil data available appear to be three data points due to Shen and Peterson [58,59] (see

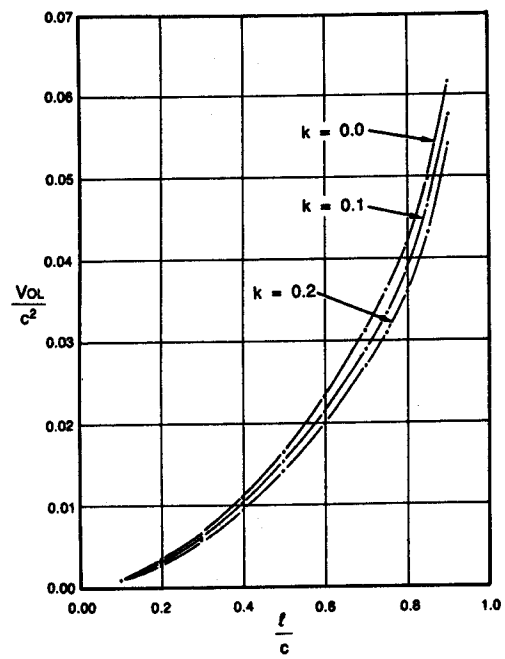

Fig. 26 VOL/c^2 versus ℓ/c, camber results, k = design lift coefficient, NACA 16-006 section and a = 0.8 meanline, α = 4 deg

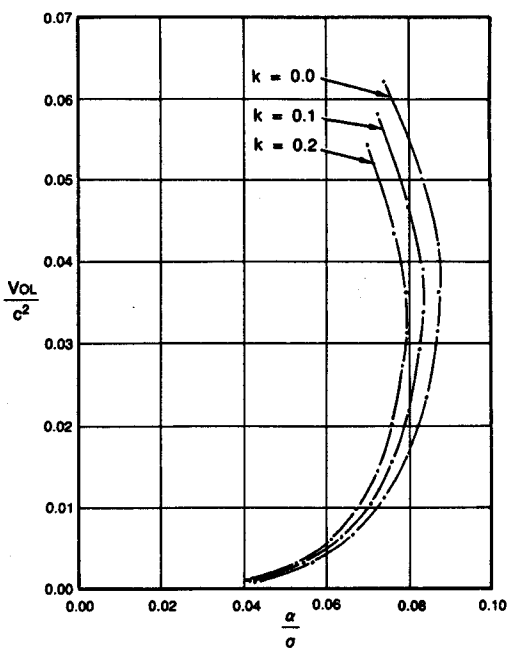

Fig. 27 VOL/c^2 versus α/σ, camber results, k = design lift coefficient, NACA 16-006 section and a = 0.8 meanline, α = 4 deg

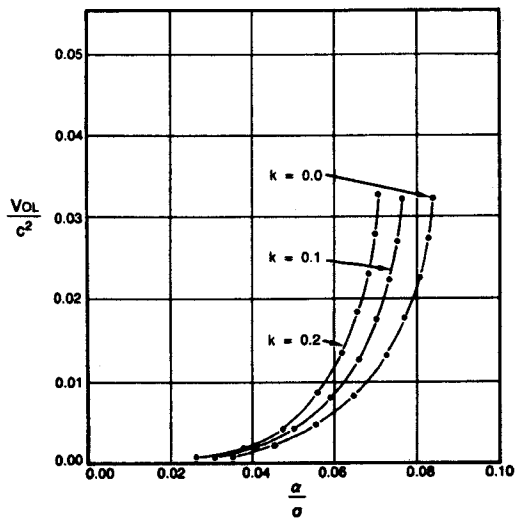

Fig. 28 VOL/c^2 versus α/σ, camber results, k = design lift coefficient, NACA 16-006 section and a = 0.8 meanline, α = 4 deg, Tulin and Hsu's results

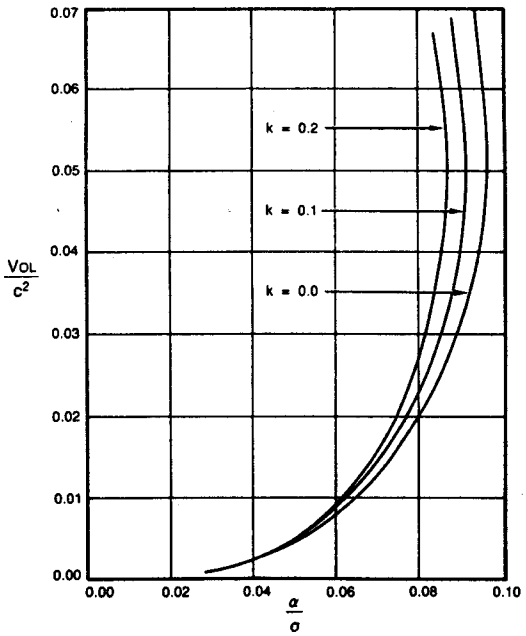

Fig. 29 VOL/c^2 versus α/σ, parabolic camber, k = design lift coefficient, α = 4 deg (Geurst and Verbrugh)

also Stern [60]). Comparisons of these experimental results with the results of the present nonlinear theory and with the results of the linear theory including thickness effects are given in Table 5. The predictions of the present nonlinear model are seen to be excellent.

Further results generated by the present nonlinear theory, particularly those concerning lift and moment coefficients, have been compiled in Appendix D of Uhlman [62]. Corresponding linear results, obtained from Geurst and Verbrugh [22] and Van Houten [42], are contained in Appendix E of the same work.

Conclusions

The present program, PCAV, which determines the potential-flow solution for the nonlinear two-dimensional partially cavitating hydrofoil problem, has been shown to converge to a single solution given a sufficient number of surface elements and a sufficient number of iterations. It has also been shown that once convergence is achieved the boundary conditions on the foil-cavity boundary are properly satisfied. Theorems in potential-flow theory then state that the unique solution has been found. The absence of any exact analytic solutions to this problem unfortunately precludes any direct comparison with the present numerical approach.

The comparison of the present nonlinear results with the numerical linear theory of Van Houten [42] brings to light several salient facts. For section thickness ratios of 6 percent or greater it is seen that the linear theory underpredicts the effect of section thickness on cavity volume. Thus linear theory significantly overpredicts the cavity volume of foils with thickness. In fact, for constant α/σ, linear theory indicates an increase of cavity volume with increasing section thickness in contradiction to the trend predicted by the present nonlinear theory. This suggests that linear theory may best be utilized by neglecting the effect of section thickness altogether. Linear theory also approaches the wrong α/σ limit for short cavities on round-nosed foils. Although the cavity volumes at these short cavity lengths are small, this indicates that any attempt at modeling inception will, of necessity, involve a nonlinear theory.

It is the author's opinion that Tulin and Hsu's theory [39] overpredicts the effect of section thickness on cavity volume. Their theory suggests that doubling the section thickness could often virtually do away with cavitation entirely. Tulin and Hsu also indicate a similar effect for camber. The present theory indicates that the effect of increased section thickness in reducing cavity volume is significant, but not as drastic as that predicted by Tulin and Hsu. Similarly, an increase in camber will also

Table 5 Comparison of experimental and numerical results for a modified Joukowski section

	ℓ/c = 0.40 α = 4.3 deg	ℓ/c = 0.30 α = 4.3 deg	ℓ/c = 0.25 α = 3.8 deg
Experiment	σ = 1.13	σ = 1.21	σ = 1.13
Nonlinear theory	1.11	1.20	1.14
Linear theory with thickness	1.37	1.53	1.51

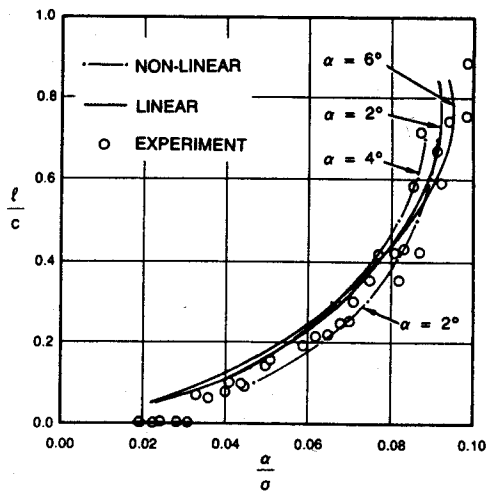

Fig. 30 Meijer's experimental data for a 4 percent bi-convex foil, α = 2 deg, 4 deg, and 6 versus nonlinear theory and linear theory

reduce cavity volume, but again not as drastically as Tulin and Hsu indicate.

Recommendations

The comparisons encountered above are between an exact nonlinear solution and various approximations. Comparison with experimental data is virtually nonexistent. However, before any theory can claim an element of truth it must be validated by comparison with experimental results. In the present case experimental results are sorely lacking. This situation must be remedied. In particular, accurate measurements of cavity volume must be obtained.

Further analytic results would also be useful. In particular, the linear theory for a partially cavitating bi-convex hydrofoil including thickness effects could be used to investigate the effect of section thickness on cavity volume and at the same time validate corresponding numerical results.

An extension of the numerical nonlinear technique to a three-dimensional hydrofoil would also be worthwhile. Such an extension would allow one to study to what extent finite span effects mediate the effects of thickness and camber on cavity volume.

In problems involving cavitation-induced vibration it is the volume velocity of the cavity, rather than the volume itself, that is of concern. Although the present theory could be readily employed in a quasi-steady analysis of such problems, an extension of the technique to time-dependent flows would be of great value.

The problem of cavitation inception is also of considerable interest. The present technique, or a similar local extension of it, could be useful in investigating this problem. However, due to the small cavity lengths and volumes involved, knowledge of the exact location of the cavity separation point would become important. Therefore some criterion for determining this location would have to be found. The development of such a criterion would presumably require a local viscous analysis about the nose of the hydrofoil.

Acknowledgments

This work—performed while the author was a student at the Massachusetts Institute of Technology—was largely supported by the Maritime Administration of the Department of Transportation. The author would like to thank Professors J. E. Kerwin and P. Leehey of M.I.T. for their support and direction in the performance of this work. Special thanks are extended to Dr. R. J. Van Houten for his assistance in the calculation of the results of the linear theory with thickness.

References

1 Birkhoff, G., and Zarantonello, E. H., *Jets, Wakes and Cavities*, Academic Press, New York, 1957.

2 Eisenberg, P. and Tulin, M. P., *Handbook of Fluid Mechanics*, V. L. Streeter, Ed., McGraw-Hill, New York, 1961.

3 Gilbarg, D., "Jets and Cavities," in *Handbuch Der Physik*, Vol. 9, Springer-Verlag, Berlin, 1960.

4 Gurevich, M. I., *Theory of Jets in Ideal Fluids*, Academic Press, New York, 1965.

5 Gurevich, M. I., "The Theory of Flow with Free Surfaces," Joint Publication Research Service Translation Report No. 56501, 1972.

6 Hsu, C. C., "Some Remarks on the Progress of Cavity Flow Studies," *Journal of Fluids Engineering, Trans.*, ASME, Vol. 97, No. 4, 1975.

7 Knapp, R. J., Daily, J. W., and Hammitt, F. G., *Cavitation*, McGraw-Hill, New York, 1970.

8 Plesset, M. S. in *Cavitation in Real Liquids*, R. Davies, Ed., Elsevier, Amsterdam, 1964.

9 *Cavitation State of Knowledge*, J. M. Robertson and G. F. Wislicenus, Eds. American Society of Mechanical Engineers, New York, 1969.

10 Tulin, M. P., "Supercavitating Flows—Small Perturbation Theory," JOURNAL OF SHIP RESEARCH, Vol. 7, No. 3, Jan. 1964, pp. 16–37.

11 Tulin, M. P. and Hsu, C. C., "New Applications of Cavity Flow Theory" in *Proceedings*, 13th Symposium on Naval Hydrodynamics, Tokyo, 1980.

12 Wehausen, J. V., "Research Frontiers in Fluid Dynamics," R. J. Seeger and G. Temple, Eds., InterScience, New York 1965.

13 Wu, T. Y., *Basic Developments in Fluid Dynamics*, M. Holt, Ed., Academic Press, New York, 1968.

14 Wu, T. Y. "Cavity and Wake Flows," *Annual Review of Fluid Mechanics*, Vol. 4, 1972.

15 Yegorov, I. T. et al, "Artificial Cavitation," Joint Publication Research Service Translation Report No. JPRS54423, 1971.

16 Shiffman, M., "On Free Boundaries of an Ideal Fluid—I," *Communications on Pure and Applied Mathematics*, 1948, pp. 89–99.

17 Shiffman, M., "On Free Boundaries of an Ideal Fluid—II," *Communications on Pure and Applied Mathematics*, 1949, pp. 1–11.

18 Gilbarg, D. and Serrin, J., "Free Boundaries and Jets in the Theory of Cavitation," *Journal of Mathematics and Physics*, Vol. 29, 1950, pp. 1–12.

19 Efros, D. A., "Hydrodynamic Theory of Two-Dimensional Flow with Cavitation," *Doklady Akademil Nauk SSSR*, Vol. 51, 1946, pp. 267–270.

20 Tulin, M. P., "Steady Two-Dimensional Cavity Flows About Slender Bodies," David Taylor Model Basin Report 834, Navy Department, Washington, D.C., May 1953.

21 Geurst, J. A., "Linearized Theory for Partially Cavitated Hydrofoils," *International Shipbuilding Progress*, Vol. 6, No. 60, August 1959.

22 Geurst, J. A. and Verbrugh, P. J., "A Note on Camber Effects of a Partially Cavitated Hydrofoil," *International Shipbuilding Progress*, Vol. 6, No. 61, Sept. 1959.

23 Geurst, J. A., "Linearized Theory for Fully Cavitated Hydrofoils," *International Shipbuilding Progress*, Vol. 7, No. 65, January 1960.

24 Wade, R. B., "Linearized Theory of a Partially Cavitating Plano Convex Hydrofoil Including the Effects of Camber and Thickness," JOURNAL OF SHIP RESEARCH, Vol. 11, No. 1, March 1967, pp. 20–27.

25 Leehey, P., "Supercavitating Hydrofoil of Finite Span" in *Proceedings*, IUTAM Symposium on Non-Steady Flow of Water at High Speeds, Leningrad, June 1971, NAUKA Publishing House, Moscow, 1973.

26 Uhlman, J. S., "A Partially Cavitated Hydrofoil of Finite Span," *Journal of Fluids Engineering, Trans.* ASME, Vol. 100, No. 3, Sept. 1978, pp. 353–354.

27 Golden, D. W., "A Numerical Method for Two-Dimensional, Cavitating Lifting Flow," Massachusetts Institute of Technology, Department of Ocean Engineering, Report No. 81512-1, Cambridge, Mass., May 1975.

28 Jiang, C. W., "Experimental and Theoretical Investigation of Unsteady Supercavitating Hydrofoils of Finite Span," Ph.D. Thesis, M.I.T., Department of Ocean Engineering, Cambridge, Mass., 1977.

29 Lee, C. S., "Prediction of Steady and Unsteady Performance of Marine Propellers With or Without Cavitation by Numerical Lifting Surface Theory," Ph.D. Thesis, M.I.T., Department of Ocean Engineering, Cambridge, Mass., May 1979.

30 Hess, J. L. and Smith, A. M. O., "Calculation of Potential Flow About Arbitrary Bodies," *Progress in Aeronautical Sciences*, Vol. 8, Pergamon Press, New York, 1966.

31 Hess, J. L., "Higher Order Numerical Solution of the Integral-Equation for the Two-Dimensional Neumann Problem," *Computer Methods in Applied Mechanics and Engineering*, North Holland Publishing Co., Amsterdam, Vol. 2, 1973, pp. 1–15.

32 Hess, J. L., "The Use of Higher-Order Surface Singularity Distributions to Obtain Improved Potential Flow Solutions for Two-Dimensional Lifting Airfoils," *Computer Methods in Applied Mechanics and Engineering*, North Holland Publishing Co., Amsterdam, Vol. 5, 1975, pp. 11–35.

33 Basu, B. C. and Hancock, G. J., "The Unsteady Motion of a Two-Dimensional Hydrofoil in Incompressible Inviscid Flow," *Journal of Fluid Mechanics*, 1978, Vol. 87, Part 1, pp. 159–178.

34 Bristow, D. R., "A New Surface Singularity Method for Multi-Element Airfoil Analysis and Design," American Institute of Aeronautics and Astronautics 14th Aerospace Sciences Meeting, AIAA Paper No. 76-20, Washington, D.C., Jan. 1976.

35 Giesing, J. P. and Smith, A. M. O., "Potential Flow about Two-Dimensional Hydrofoils," *Journal of Fluid Mechanics*, Vol. 28, Part 1, 1967, pp. 113–129.

36 Hess, J. L., "Progress in the Calculation of Non-Linear Free-Surface Problems by Surface Singularity Techniques," in *Proceedings*, Second International Conference on Numerical Ship Hydrodynamics, 1977, pp. 278–284.

37 Larock, B. E., "An Application of the Boundary Integral Equa-

tion Method to Cavity and Jet Flows," in *Proceedings*, Second International Conference on Numerical Ship Hydrodynamics, 1977, pp. 269–274.
38 Pellone, E. and Rowe, A., "Supercavitating Hydrofoils in Non-Linear Theory" in *Proceedings*, Third International Conference on Numerical Ship Hydrodynamics, 1981.
39 Tulin, M. P. and Hsu, C. C., "The Theory of Leading-Edge Cavitation on Lifting Surfaces with Thickness" in *Proceedings*, Symposium on Hydrodynamics of Ship and Offshore Propulsion Systems, March 1977.
40 Arakeri, V. H., "Viscous Effects on the Position of Cavitation Separation from Smooth Bodies," *Journal of Fluid Mechanics*, Vol. 68, Part 4, 1975, pp. 779–799.
41 Meijer, M. C., "Some Experiments on Partly Cavitating Hydrofoils," *International Shipbuilding Progress*, Vol. 6, No. 60, Aug. 1959.
42 Van Houten, R. J., "The Numerical Prediction of Unsteady Sheet Cavitation on High Aspect Ratio Hydrofoils" in *Proceedings*, Fourteenth Symposium on Naval Hydrodynamics, 1982.
43 Persson, E., "Theoretical Study of Cavitation on a Flat Plate," Det norske Veritas Technical Report 78/440, Oslo, 1978.
44 Wade, R. B. and Acosta, A. J., "Experimental Observations on the Flow Past a Plano-Convex Hydrofoil," *Journal of Basic Engineering*, March 1966.
45 Uhlman, J. S. and Jiang, C. W., "Experiments on a Partially Cavitating Plano-Convex Hydrofoil with Comparison to Theory," M.I.T., Department of Ocean Engineering, Report No. 83481-2, Cambridge, Mass., July 1977.
46 Lamb, H., *Hydrodynamics*, 6th ed., Dover Publications, New York, 1932.
47 Hess, J. L., "Review of Integral-Equation Techniques for Solving Potential-Flow Problems with Emphasis on the Surface Source Method," *Computer Methods in Applied Mechanics and Engineering*, North Holland Publishing Co., Amsterdam, Vol. 5, 1975, pp. 145–196.
48 Lin, W., "Solution of Single- or Multi-Foil Problems by Surface-Vortex Distribution Based on Linear Elemental Variation," Master's Thesis, M.I.T., Department of Ocean Engineering, Cambridge, Mass., 1981.
49 Baker, G. R., Meiron, D. I., and Orszag, S. A., "Applications of a Non-Linear Free-Surface Flows" in *Proceedings*, Third International Conference on Numerical Ship Hydrodynamics, 1981.
50 Johnson, F. T. and Ruppert, P. E., "Advanced Panel-Type Influence Coefficient Method Applied to Subsonic Flows," American Institute of Aeronautics and Astronautics 13th Aerospace Sciences Meeting, AIAA Paper No. 75-50, Pasadena, Calif., Jan. 1975.
51 Hunt, B., "The Panel Method for Subsonic Aerodynamic Flows: A Survey of Mathematical Formulations and Numerical Models and an Outline of the New British Aerospace Scheme," *Computational Fluid Dynamics*, W. Kollman, Ed., Hemisphere Publishing, Washington, D.C., 1980.
52 Brennen, C., "A Numerical Solution of Axisymmetric Cavity Flows," *Journal of Fluid Mechanics*, Vol. 37, Part 4, 1969, pp. 671–688.
53 Wu, T. Y., "Cavity Flow and Numerical Methods" in *Proceedings*, First International Conference on Numerical Ship Hydrodynamics, 1976.
54 Furuya, O. and Acosta, A. J., "A Note on the Calculation of Supercavitating Hydrofoils with Rounded Noses," *Journal of Fluids Engineering, Transactions*, American Society of Mechanical Engineers Vol. 95, No. 2, June 1973.
55 Plotkin, A., "Leading-Edge Correction for the Supercavitating Flat-Plate Hydrofoil," *Journal of Fluids Engineering*, Vol. 100, Sept. 1978, pp. 276–280.
56 Kerwin, J. E., Private communication, 1982.
57 Geurst, J. A., "Linearized Theory for Fully Cavitated Hydrofoils," *International Shipbuilding Progress*, Vol. 7, No. 65, Jan. 1960.
58 Shen, Y. T. and Peterson, F. B., "Unsteady Cavitation on an Oscillating Hydrofoil" in *Proceedings*, Twelfth Symposium on Naval Hydrodynamics, Washington, D.C., June 1978.
59 Shen, Y. T. and Peterson, F. B., "Influence of Hydrofoil Oscillation on Boundary Layer Transition and Cavitation Noise" in *Proceedings*, 13th Office of Naval Research Symposium on Naval Hydrodynamics, Tokyo, Oct. 1980.
60 Stern, F., "Comparison of Computational and Experimental Unsteady Sheet Cavitation," in *Proceedings*, 14th Symposium on Naval Hydrodynamics, Ann Arbor, Mich., Aug. 1982.
61 Dong, S., "A Theoretical Solution of Partially Cavitating Flow Past A Hydrofoil with Thickness," *Transactions*, Chinese Society of Naval Architects and Marine Engineers, No. 80, Jan. 1983.
62 Uhlman, J. S., "The Surface Singularity Method Applied to Partially Cavitating Hydrofoils," Ph.D. Thesis, Massachusetts Institute of Technology, Department of Ocean Engineering, Cambridge, Mass., 1983.

Appendix

On the Representation of the Velocity Field by a Distribution of Vortices Over the Boundary

Consider the steady flow of an unbounded ideal fluid past a closed two-dimensional body. Such a flow may be described by a velocity potential, Γ. One may then introduce a disturbance velocity potential, ϕ, such that

$$\Phi = \vec{U} \cdot \vec{r} + \phi \tag{78}$$

where $\vec{U}$ represents the freestream velocity and $\vec{r} = x\vec{i} + y\vec{j}$ is the position vector. This disturbance potential satisfies the condition that

$$\phi \to 0 \qquad \text{as} \qquad r \to \infty \tag{79}$$

Hence, from Green's second identity it can be shown that ϕ may be represented by distributions over the fluid boundary, ∂D, of sources and normal dipoles of the form

$$\phi = \frac{1}{2\pi} \int_{\partial D} \left\{ \frac{\partial \phi}{\partial n} \ell n(r) - \phi \frac{\partial [\ell n(r)]}{\partial n} \right\} ds \tag{80}$$

If the circulation about the body is zero, then ϕ may be expressed as a unique distribution of solely sources or a unique distribution of solely normal dipoles (see Lamb [46], pp. 59–61).

If, however, the circulation about the body is nonzero, then the velocity potential becomes multivalued and a barrier or auxiliary flow boundary must be introduced into the fluid to render it single-valued once again (see Fig. 31). In fact, the circulation about the body is

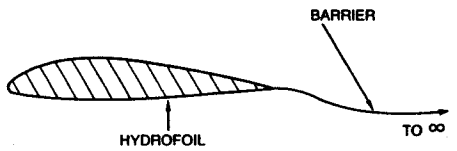

Fig. 31

exactly equal to the jump in potential across this barrier. Thus, if ϕ is to be expressed in terms of boundary distributions of sources and normal dipoles, then there must exist a constant distribution of normal dipoles on the barrier with the density of the dipole moment equal to the circulation.

It is no longer possible to express ϕ solely in terms of sources. It is, however, possible to use Lamb's interior flow arguments to express ϕ in terms of normal dipoles alone. Thus

$$\phi = \frac{-1}{2\pi} \int_{\partial D} (\phi - \tilde{\phi}) \frac{\partial}{\partial n} [\ell n(r)] ds + \frac{\Delta \phi}{2\pi} \int_B \frac{\partial}{\partial n} [\ell n(r)] ds \tag{81}$$

where $\tilde{\phi}$ is the potential in domain D^- such that

$$\frac{\partial \tilde{\phi}}{\partial n} = \frac{\partial \phi}{\partial n} \qquad \text{on } \partial D \tag{82}$$

and $\Delta\phi$ is the jump in potential across the barrier. One may now introduce the multivalued function

$$\Theta(x,y) = \arctan(y/x) \tag{83}$$

This is the conjugate harmonic function of $\ell n(r)$ and hence the Cauchy-Riemann equations state that

$$\frac{\partial}{\partial n} [\ell n(r)] = \frac{\partial \Theta}{\partial s} \tag{84}$$

Equation (81) may therefore be written as

$$\phi = \frac{1}{2\pi} \int_{\partial D} (\phi - \tilde{\phi}) \frac{\partial \Theta}{\partial s} (x - \xi, y - \eta) ds + \frac{\Delta \phi}{2\pi} \int_B \frac{\partial \Theta}{\partial s} (x - \xi, y - \eta) ds \tag{85}$$

One may perform an integration by parts on equation (8) to yield

$$\phi = \frac{1}{2\pi}\int_{\partial D}\frac{\partial}{\partial s}(\phi - \tilde{\phi})\Theta ds \tag{86}$$

which expresses the velocity potential in terms of a distribution of vortices over the body boundary ∂D. The barrier now serves the purpose of defining which branch of the multivalued function Θ is under consideration.

The simplest manner of demonstrating that the flow about a body with nonzero circulation can be represented in terms of a boundary distribution of vortices alone is to consider the stream function Ψ. If U and V denote the x and y components of the free stream, respectively, then one may define a disturbance stream function, ψ, by

$$\Psi = (Uy - Vx) + \psi \tag{87}$$

This disturbance stream function satisfies the conditions necessary to apply Green's second identity and hence may be written as

$$\psi = \frac{1}{2\pi}\int_{\partial D}\left\{\frac{\partial \psi}{\partial n}\ell n(r) - \psi\frac{\partial}{\partial n}[\ell n(r)]\right\}ds \tag{88}$$

The above representation expresses Ψ in terms of boundary distributions of vortices and tangential dipoles. If there is no flux from the body boundary, then the body boundary is a streamline and the stream function is single-valued. The arguments of Lamb concerning interior flows may then be applied. In particular, consider an interior stream function $\tilde{\psi}$. In the region D^+, $\tilde{\psi}$ satisfies

$$0 = \frac{1}{2\pi}\int_{\partial D}\left\{\frac{\partial \tilde{\psi}}{\partial \tilde{n}}\ell n(r) - \tilde{\psi}\frac{\partial}{\partial \tilde{n}}[\ell n(r)]\right\}ds \tag{89}$$

where $\partial/\partial\tilde{n} = \partial/\partial n$. If one now requires that

$$\tilde{\psi} = \psi \qquad \text{on } \partial D \tag{90}$$

then equations (89) and (90) may be combined to yield

$$\psi = \frac{1}{2\pi}\int_{\partial D}\left\{\frac{\partial \tilde{\psi}}{\partial n} - \frac{\partial \tilde{\psi}}{\partial n}\right\}\ell n(r)ds, \qquad \text{in } D^+ \tag{91}$$

which was to be shown.

It should be noted that whether or not the velocity potential (or stream function) is multivalued, the associated velocity field is single-valued. Hence, since the present work deals only with velocities, the question of multivaluedness does not arise.